(12)

RADC-TR-82-274
In-House Report
October 1982

SIMULTANEOUS NULLING IN THE SUM AND DIFFERENCE PATTERNS OF A MONOPULSE ANTENNA

Randy L. Haupt, Captain, USAF

ROME AIR DEVELOPMENT CENTER
Air Force Systems Command
Griffiss Air Force Base, NY 13441

This report has been reviewed by the RADC Public Affairs Office (PA) and is releasable to the National Technical Information Service (NTIS). At NTIS it will be releasable to the general public, including foreign nations.

RADC-TR-82-274 has been reviewed and is approved for publication.

APPROVED: J. Leon Poirier

J. LEON POIRIER
Acting Chief, EM Techniques Branch
Electromagnetic Sciences Division

APPROVED: Allan C. Schell

ALLAN C. SCHELL
Chief, Electromagnetic Sciences Division

FOR THE COMMANDER: John P. Huss

JOHN P. HUSS
Acting Chief, Plans Office

If your address has changed or if you wish to be removed from the RADC mailing list, or if the addressee is no longer employed by your organization, please notify RADC (EEC), Hanscom AFB MA 01731. This will assist us in maintaining a current mailing list.

Do not return copies of this report unless contractual obligations or notices on a specific document requires that it be returned.

Unclassified

SECURITY CLASSIFICATION OF THIS PAGE (When Data Entered)

REPORT DOCUMENTATION PAGE		READ INSTRUCTIONS BEFORE COMPLETING FORM
1. REPORT NUMBER RADC-TR-82-274	2. GOVT ACCESSION NO. AD-A131 865	3. RECIPIENT'S CATALOG NUMBER
4. TITLE (and Subtitle) SIMULTANEOUS NULLING IN THE SUM AND DIFFERENCE PATTERNS OF A MONOPULSE ANTENNA		5. TYPE OF REPORT & PERIOD COVERED In-House 6. PERFORMING ORG. REPORT NUMBER
7. AUTHOR(s) Randy L. Haupt, Capt, USAF		8. CONTRACT OR GRANT NUMBER(s)
9. PERFORMING ORGANIZATION NAME AND ADDRESS Electromagnetic Sciences Division (RADC/EEC) Hanscom AFB Massachusetts 01731		10. PROGRAM ELEMENT, PROJECT, TASK AREA & WORK UNIT NUMBERS 62702F 46001507
11. CONTROLLING OFFICE NAME AND ADDRESS Electromagnetic Sciences Division (RADC/EEC) Hanscom AFB Massachusetts 01731		12. REPORT DATE October 1982 13. NUMBER OF PAGES 105
14. MONITORING AGENCY NAME & ADDRESS(if different from Controlling Office)		15. SECURITY CLASS. (of this report) Unclassified 15a. DECLASSIFICATION/DOWNGRADING SCHEDULE

16. DISTRIBUTION STATEMENT (of this Report)

Approved for public release; distribution unlimited.

17. DISTRIBUTION STATEMENT (of the abstract entered in Block 20, if different from Report)

18. SUPPLEMENTARY NOTES

RADC Project Engineer: Randy L. Haupt, Captain, USAF, RADC/EEC

19. KEY WORDS (Continue on reverse side if necessary and identify by block number)

Adaptive antenna
Nulling
Monopulse antenna

20. ABSTRACT (Continue on reverse side if necessary and identify by block number)

Most adaptive array research neglects the problem of nulling in a monopulse antenna. Placing a null in the sum pattern does not automatically place a null in the difference pattern and vice versa. Nulls may be placed in the two patterns by having separate adaptive weights and controls for each channel, however, this method uses two sets of adaptive hardware for one antenna. This paper develops a technique for simultaneous nulling in the sum and difference patterns of a monopulse phased array using one set of adaptive weights shared by both channels. First, the technique is used for amplitude and phase nulling

DD FORM 1 JAN 73 1473 EDITION OF 1 NOV 65 IS OBSOLETE

Unclassified

SECURITY CLASSIFICATION OF THIS PAGE (When Data Entered)

20. (Contd)

then for phase-only nulling. In each case, the ability to simultaneously null in both channels with one set of weights, chosen to place a null at a particular location, is theoretically demonstrated.

Contents

Illustrations

Illustrations

Tables

Simultaneous Nulling in the Sum ar Difference Patterns of a Monopt Antenna

1. INTRODUCTION

In the past few years, considerable research and development has been expended on adaptive antennas. Communications and sonar systems have reaped some of the benefits of adaptive technology while radars generally lag behind. Some of the reasons for this dichotomy are that many adaptive techniques are not suited for microwave frequencies; that phased array radars are large with many antenna elements, hence more adaptive loops are required; and that a radar has tight time constraints for detecting and tracking targets which necessitates the use of fast response adaptive loops. Consequently, only a handful of radars incorporating sidelobe cancelling techniques exist today.

Monopulse radars add additional problems in the implementation of adaptive processing. The problems stem from the coexistence of a sum and difference pattern. A monopulse phased array antenna uses two antenna patterns: one to detect and range a target and a second to determine a target's angular location. Most adaptive antenna research has not directly addressed nulling for both these patterns, even though both patterns must have a null in the direction of interference to enhance the radar's performance. Adjusting the far field sum pattern to place a null in the direction of interference will not place a null in the difference pattern too.

(Received for publication 8 December 1982)

Hence, either the sum and difference channels must be adapted separately or a technique of simultaneously nulling in both channels can be used. Current approaches to this problem have usually assumed the first approach, and the possibility of simultaneous nulling has not been investigated.

This report has a dual purpose. First, it describes the problem of nulling in monopulse antennas and points out that both the sum and difference channels need to be considered in the design of the adaptive processing system. And second, it theoretically demonstrates that nulls can be placed simultaneously in the sum and difference patterns of a monopulse phased array antenna using one set of adaptive weights shared by the two channels. The technique used to generate these nulls offers significant hardware and software savings over current methods.

The next section of this report introduces the concepts used in array analysis and synthesis. It covers linear array analysis, sum and difference patterns, unit circle representation, and low sidelobe synthesis. This section provides the background and notation necessary for understanding the nulling techniques introduced later.

The following two sections deal with nulling in sum and difference channels. Section 3 performs the nulling using phase and amplitude weights while Section 4 shows a method for phase-only nulling. Both techniques are demonstrated for the sum channel, then the difference channel, and finally simultaneous nulling in both channels.

Section 5 explains the computer program used to demonstrate the above analysis and shows several results.

The final section outlines the pros and cons of using the techniques described. In addition, it discusses the practical implementation of this method and future work needed.

2. ARRAY ANALYSIS AND SYNTHESIS

This section describes the basic concepts required to understand array analysis and synthesis. The theory provides the basic tools needed to tackle the nulling problem analyzed in the following sections. A great deal of the information presented here was drawn from array antenna books by Elliot and Steinberg.[1,2] The reader is referred to these books for additional information.

---

1. Elliot, Robert S. (1981) Antenna Theory and Design, Prentice-Hall, Inc., Englewood Cliffs, N.J.
2. Steinberg, B.D. (1976) Principles of Aperture and Array System Design, John Wiley, New York.

Consider a linear array with N isotropic, equally spaced (d_o) radiating elements (Figure 1). Each element receives signals from sources in its environment. The signals pass through a phase shifter and amplitude weight to a summer. The summer adds all the signals together to generate one output signal. Adjusting the phase and amplitude of the received signals can enhance a desired signal by rejecting unwanted signals.

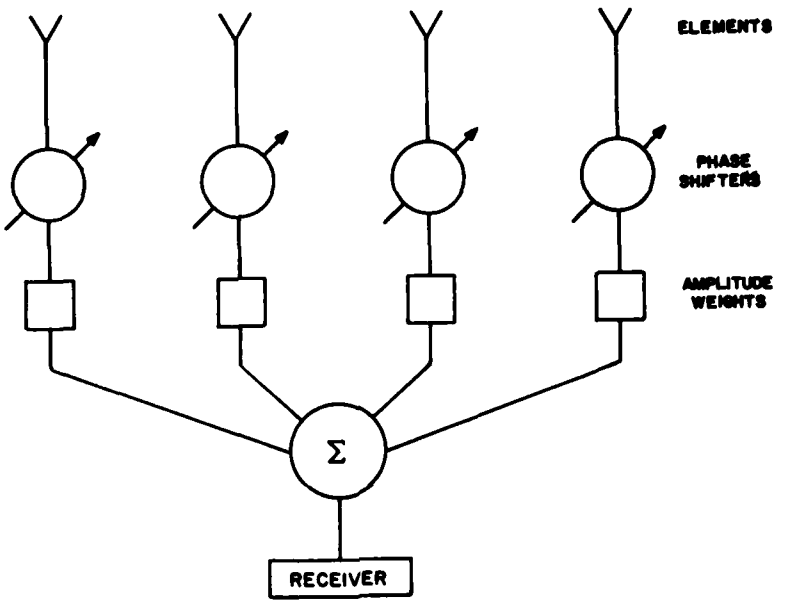

Figure 1. Linear Array of N Elements

A point source very far from the antenna produces a uniform plane wave across the face of the aperture. If the source is at broadside ($\theta = 0°$), then each element sees the same signal phase and amplitude. As θ changes, so does the phase seen by each element.

The difference in phase between two elements (m, n) is

$$\Delta\theta_{m,n} = k\ell_{m,n} \tag{1}$$

where

k = propagation constant = $2\pi/\lambda$

λ = wavelength

$\ell_{m,n}$ = the additional distance the uniform plane wave must travel from the time it reaches element m until reaching element n.

If the physical center of the array is also the phase center, then the phase of the signal at element n is is

$$\xi_n = \frac{2\pi}{\lambda} d_o [n - (N/2) - 0.5] \sin\theta \tag{2a}$$

$$= d_n \sin\theta = d_n u \tag{2b}$$

$$d_n = k d_o [n - (N/2) - 0.5] . \tag{3}$$

All the element outputs of the phased array are summed together to generate one output. At broadside, all the signals are equal, so the output is equal to N times the signal level at one element. If the signal source is moved in an arc around the array (or the antenna rotated) the output of the summer will vary. The phase of the signal at each element changes by $\frac{2\pi}{\lambda} d_o \sin\theta$ as θ varies. Therefore, the signals do not add in phase. In fact, as θ increases, a point is reached where all the signals added together totally cancel and result in a null. The output graphs an interference pattern from $\theta = -90°$ to $\theta = +90°$. This far field antenna pattern is represented by the summation of the signal amplitude and phase at each element

$$S(u) = \sum_{n=1}^{N} e^{j d_n u} . \tag{4}$$

The mainbeam lies between the first null in the θ direction and the first null in the $-\theta$ direction. Continuing to increase θ produces a series of nulls and peaks. The peaks are called sidelobes and are usually much smaller than the mainbeam.

The maximum output from the summer occurs when all the signals entering the summer have the same phase. Normally, this condition occurs only when the source is at broadside. However, the signal phase at each element may be changed by a phase shifter. Applying a phase shift of $-\phi_n$ at each element causes all the signals to have the same phase so that they add up to a maximum value when the source is at some angle θ away from broadside. In effect, the linear phase shift of $-\phi_n$ steers the mainbeam in the direction of the desired source. The far field pattern of the steered beam is

$$S(u) = \sum_{n=1}^{N} e^{j(d_n u - \phi_n)} . \tag{5}$$

When the signals at each element are added in phase, a sum pattern is formed. A monopulse radar uses this pattern to detect and determine the range of a target. To track a target, a monopulse radar uses a difference pattern. The difference pattern has a null at $\theta = 0°$. It is formed by giving the signals from half of the array elements a 180° phase shift and adding them to the element signals from the other half of the array. The resultant pattern has a different sidelobe and null structure than the sum pattern. Like the sum beam, the difference beam can be steered to a given direction by placing a linear phase shift, $-\phi_n$, across the array. The far field difference pattern (N even) is represented by

$$D(u) = \sum_{n=1}^{N/2} e^{j(d_n u - \phi_n)} - \sum_{n=\frac{N}{2}+1}^{N} e^{j(d_n u - \phi_n)} \tag{6}$$

The sidelobe level of the sum and difference patterns are controlled by weighting the signal amplitudes at each element. Equation (5) applies to a uniformly weighted aperture. The first sidelobe is 13.5 dB below the peak of the mainbeam. A difference pattern with a uniform amplitude distribution has a first sidelobe at 9.5 dB below the peak of the mainbeam. Throughout this paper, all sidelobe levels will be referenced to the peak power of the far field array pattern. The far field pattern of a weighted aperture is:

$$S(u) = \sum_{n=1}^{N} a_n e^{j(d_n u - \phi_n)} , \tag{7}$$

$$D(u) = \sum_{n=1}^{N} b_n e^{j(d_n u - \phi_n)} , \tag{8}$$

where a_n = sum amplitude weight at element n, and

b_n = difference amplitude weight at element n. b_n is positive when $n < N/2$ and negative when $n > N/2 + 1$.

The sidelobe reduction is not without cost. Tapering the sum amplitude distribution lowers the antenna's main beam gain.

$$\text{GAIN} = \frac{\left(\sum_{n=1}^{N} a_n\right)^2}{\sum_{n=1}^{N} a_n^2} . \tag{9}$$

In most cases the reduction in gain is small and the lowering of the sidelobes essential.

A useful array analytical technique is the unit circle representation (Figure 2). The circle has a radius of one and is centered at the origin of the real and imaginary axes. This circle is used to synthesize a far field antenna pattern in the same way a filter response is designed from a pole-zero diagram.

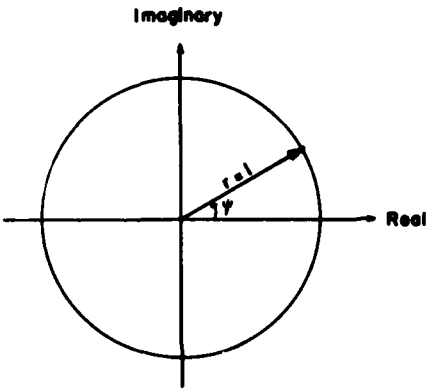

Figure 2. Unit Circle

Equation (5) represents the far field sum pattern. Let

$$s = e^{j\psi} \tag{10}$$

and

$$\psi = kd_o \sin\theta .$$

Substituting these values into the equation yields

$$S(u) = \sum_{n=1}^{N} a_n s^{(n-1)} \tag{11}$$

$$= s^{N-1} + \frac{a_{N-1}}{a_N} s^{N-2} + \ldots \frac{a_2^2}{a_N} s + \frac{a_1}{a_N} . \tag{12}$$

The fundamental theorem of algebra says a polynomial p(s) with N -1 roots can be factored into the form

$$p(s) = (s - s_1)(s - s_2)(s - s_3) \ldots (s - s_{N-1}) . \tag{13}$$

The polynomial p(s) represents the relative far field pattern of an array. The N - 1 roots, s_1, s_2, ... $s_{N=1}$, are the locations of the nulls in the far field antenna pattern. This means the angular location of the nulls is given by

$$\theta_n = \sin^{-1} (\psi_n / kd_o) . \tag{14}$$

More importantly, the coefficients of the polynomial, a_n/a_N are the amplitude weights at each element in the array.

The angles ψ determine the location of the zeros on the unit circle. This representation gives a graphical description of the antenna pattern without transforming to the far field. Zeros on the unit circle correspond to nulls in the pattern. Approximately half way between two zeros is a lobe. The farther the zeros are separated, the higher the lobe.

Consider a uniformly excited array with four elements. The far field pattern is

$$S(u) = p(s) = s^3 + s^2 + s + 1 \tag{15}$$

$$= (s + 1)(s + j)(s - j) \tag{16}$$

$$s_1 = e^{j\psi_1} = -1 \qquad \psi_1 = \pi$$

$$s_2 = e^{j\psi_2} = -j \qquad \psi_2 = 3\pi/2$$

$$s_3 = e^{j\psi_3} = j \qquad \psi_3 = \pi/2$$

As long as the coefficients of p(s) are real, the roots occur in complex conjugate pairs. An even number of elements always has a root at $\psi = \pi$. Figures 3a and 3b show the unit circle representation for this array and its corresponding far field pattern.

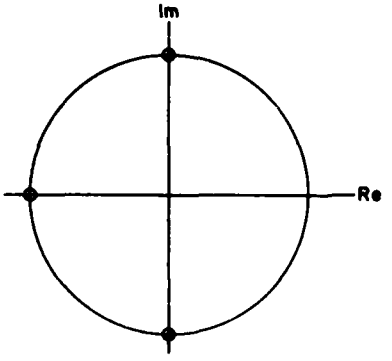

Figure 3a. Unit Circle Representation of a Four-Element Uniform Array

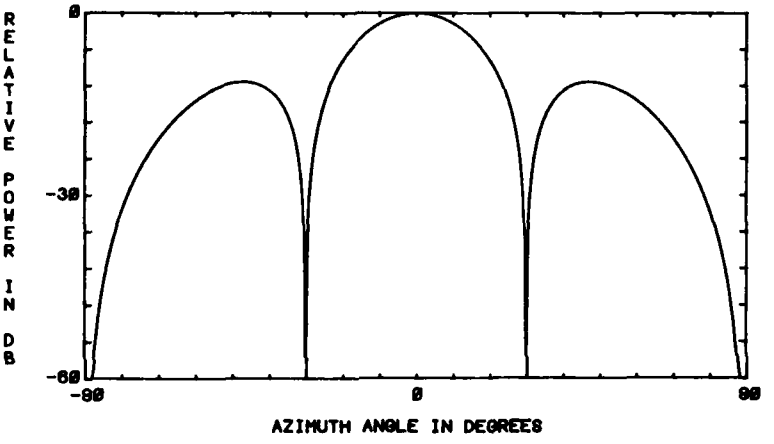

Figure 3b. Far Field Pattern of a Four-Element Uniform Array

A difference pattern may be analyzed in a similar fashion. Consider an array with the far field pattern

$$D(u) = p(s) = s^5 + 0.41\,s^4 + 0.59\,s^3 - 0.59\,s^2 - 0.41\,s - 1 \qquad (17)$$

$$= (s - e^{j3\pi/4})(s - e^{-j3\pi/4})(s - e^{-j\pi/2})(s - e^{j\pi/2})(s - e^{j0}) . \qquad (18)$$

The zeros of the pattern occur when $\psi = 3\pi/4, -3\pi/4, \pi/2, -\pi/2, 0$. Sidelobe peaks are approximately at $\pi/4, -\pi/4, 5\pi/8, -5\pi/8$. A diagram of the unit circle representation and its far field pattern are shown in Figures 4a and 4b respectively. Difference patterns always have a zero at $\psi = 0°$.

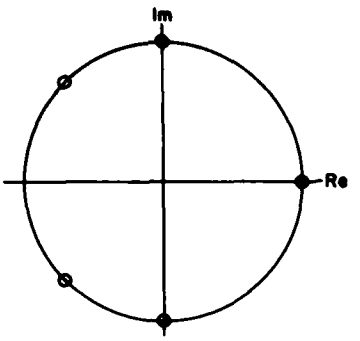

Figure 4a. Unit Circle Representation of a Six-Element Difference Array

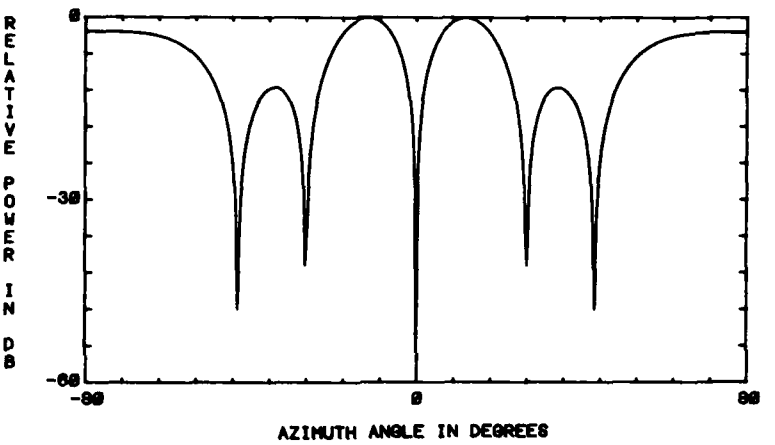

Figure 4b. Far Field Pattern of a Six-Element Difference Array

Although the past two examples demonstrate the use of the unit circle for array analysis, the technique is generally difficult to use. Arrays larger than four elements present problems with factoring the polynomial p(s). However, the unit circle is very useful in array synthesis.

If a zero indicates a null location in the pattern, and the sidelobe level is a function of the distance between two adjacent zeros, then it follows that by maneuvering the zeros on the unit circle, one can control null locations and sidelobe levels. Moving the zeros closer together in one area separates zeros farther apart in other areas. To make all the sidelobes lower, all the zeros are moved closer to the negative real axis as shown in Figure 5a. Doing this, however, increases the distance between the first two zeros on either side of the positive real axis. These zeros

determine the width of the mainbeam. Thus, the farther the zeroes are separated from the positive real axis, the lower the sidelobes and the fatter the mainbeam.

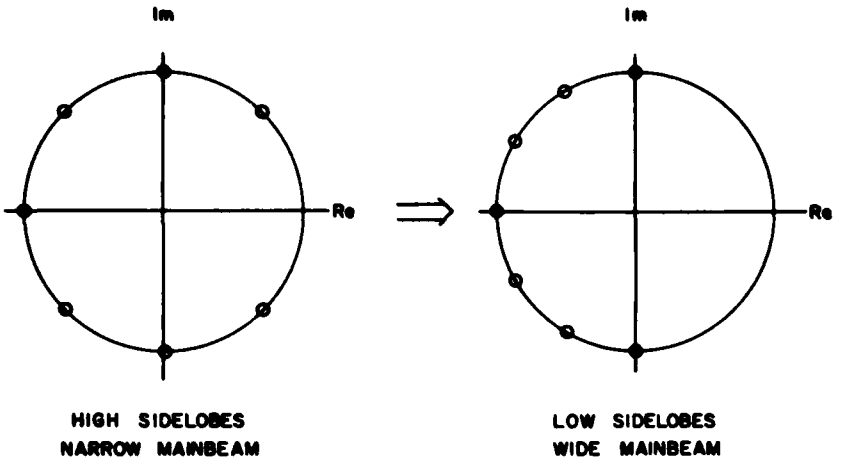

Figure 5a. Moving the Zeros on the Unit Circle to Get Lower Sidelobes

The far field antenna pattern behaves like a squeezed balloon. The part of the balloon that is squeezed goes down, while other parts of the balloon expand. "Squeezing" an antenna pattern means closely spacing the zeros on a unit circle without adding any new zeros. The sidelobes go down where the pattern is squeezed, but other parts of the pattern expand. In the case of a low sidelobe distribution all the sidelobes are "squeezed", so the mainbeam bulges.

For instance, we can move the zeroes of the four element uniform array closer to the negative real axis, which will lower the pattern's sidelobes and widen the mainbeam. Null locations at $\psi = \pm\ 3\pi/4$ instead of $\psi = \pm\ \pi/2$ give a far field pattern of

$$S(u) = (s - e^{j3\pi/4})\,(s - e^{-j3\pi/4})\,(s + 1) \tag{19}$$

$$= s^3 + 2.4\,s^2 + 2.4\,s + 1\ . \tag{20}$$

The amplitude weights are 1, 2.4, 2.4, and 1. These weights give the far field pattern shown in Figure 5b. This diagram confirms our prediction.

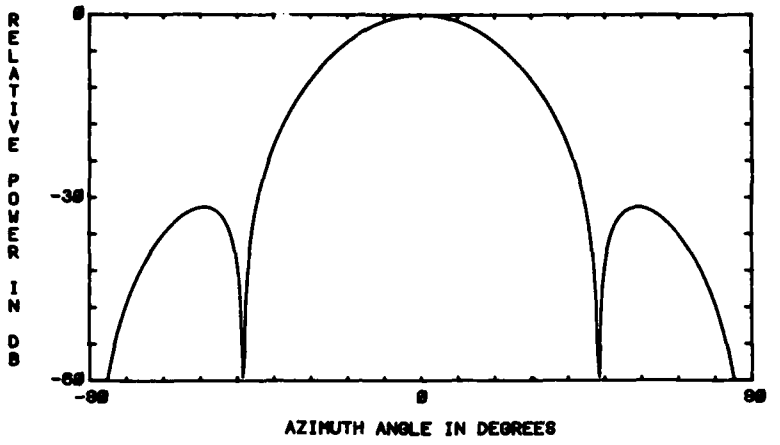

Figure 5b. Far Field Pattern of a Four-Element Array When the Zeros Are Moved on the Unit Circle

Placing zeros in certain predetermined locations can control the sidelobes. Of particular interest is the ability to specify sidelobe level and/or width of the mainbeam. Some important low sidelobe sum pattern distributions are Chebychev, Taylor, Gaussian, Cosine, and $(1 - r^2)^P$. The Bayliss distribution is the most important low sidelobe difference pattern distribution. The next few pages describe how to generate low sidelobe linear array distributions using the unit circle. Only the Chebychev, Taylor, and Bayliss distributions are considered.

The Chebychev distribution gives sidelobes of equal height for the narrowest possible mainbeam. The sidelobe level may be specified. Chebychev polynomials are the basis for the distribution. The polynomials are characterized by equal ripples of a specific heignt. Forcing the far field pattern to correspond to the polynomials will produce the desired results. The Chebychev polynomials are given by

$$T_k(u) = \cos(k\cos^{-1} v) \qquad -1 \leq u \leq 1 \tag{21}$$

$$T_k(u) = \cosh(k\cos^{-1} v) \qquad |u| \geq 1 . \tag{22}$$

Making the variable v correspond to the angle u will relate the antenna pattern S(u) to the polynomial $T_k(v)$.

The following equations perform the necessary transformation. [1]

$$T_k(u_o) = b \tag{23}$$

$$b = 10^{(\text{Desired sidelobe level}/20)} \tag{24}$$

$$u_o = \cosh \left\{ \frac{1}{N-1} [\cosh^{-1}(b)] \right\} \tag{25}$$

$$u_r = \cos \left\{ (2r-1)\,\pi / [2(N-1)] \right\} \tag{26}$$

$$\psi_r = 2 \cos^{-1} (u_r / u_o) . \tag{27}$$

When the number of elements and sidelobe level are specified, the null locations on the unit circle are easily determined. Since the values of ψ are known, the polynomial p(s) in factored form can easily be determined. Multiplying all the terms together gives a polynomial of degree N - 1. The coefficients of the s terms are the amplitude weights for the array elements.

For example, consider a six-element array with -20 dB sidelobes.

$$b = 10^{(20/20)} = 10$$

$$v_o = \cosh \left\{ \frac{1}{5} [\cosh^{-1}(10)] \right\} = 1.1846$$

$$v_r = \pm\, 0.951, \pm\, 0.588, 0$$

$$\psi = \pm\, 73.2°, \pm\, 120.5°, 180° .$$

Next, write out p(s) in factored form.

$$p(s) = \left(s - e^{j73.2°}\right)\left(s - e^{-j73.2°}\right)\left(s - e^{j120.5°}\right)\left(s - e^{-j120.5°}\right)\left(s - e^{j180°}\right) \tag{28}$$

Multiplying these factors together yields

$$p(s) = s^5 + 144^{s4} + 1.85s^3 + 1.85s^2 + 1.44\,s + 1 . \tag{29}$$

The coefficients of p(s) are the amplitude weights for the array in Figure 1. This array has the far field antenna pattern shown in Figure 6.

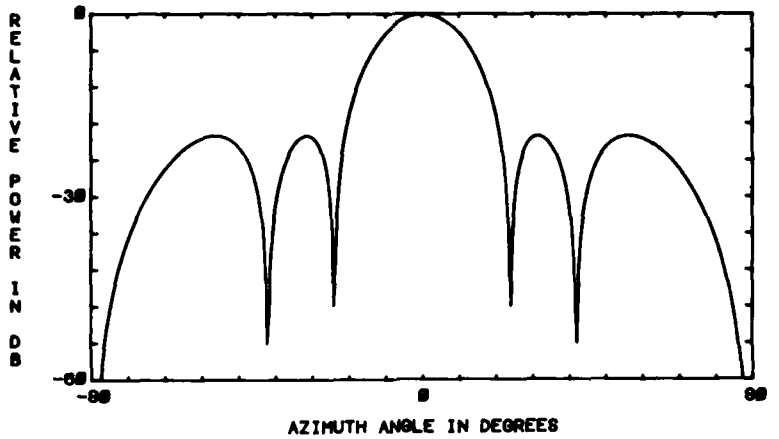

Figure 6. Far Field Pattern of a Six-Element Linear Array With a 20 dB Chebychev Taper

The Chebychev weighting is practical only for a small linear array. As N becomes large, the amplitude weightings at the edge of the aperture become large and cause mutual coupling problems due to edge effects. Other amplitude distributions are better suited for large arrays.[3]

One such distribution was developed by Taylor.[4] The Taylor distribution was originally developed for continuous line sources. However, the technique may be extended to linear and planar arrays. For a linear array, the line source is sampled to arrive at the amplitude weights at each element. A technique for deriving the element weights for a Taylor distribution is explained below.

The Taylor distribution is similar to the Chebychev distribution in that the maximum sidelobe level can be specified. The difference is that the Taylor distribution only has the first $\bar{n} - 1$ sidelobes on either side of the mainbeam at a specified height. All remaining sidelobes decrease exponentially away from the mainbeam.

The Taylor distribution may be thought of as a uniform distribution with the first $\bar{n} - 1$ zeros on the unit circle moved. The low sidelobes are obtained by moving these zeros closer to the negative real axis. Since the other zeros remain untouched, the outer sidelobes decrease exponentially, like the pattern for a uniform distribution. The new null locations are given by the formula[1]

---

3. Skolnik, Merrill L. (1980) Introduction to Radar Systems, McGraw-Hill Book Co., New York.

4. Taylor, T. T. (1955) Design of line-source antennas for narrow beamwidth and low sidelobes, IRE Transactions-Antennas and Propagation, AP-3:16-28.

$$u_n = \begin{cases} \bar{n}\left[\dfrac{A^2 + (n-0.5)^2}{A^2 + (\bar{n}+0.5)^2}\right]^{1/2} & (n < \bar{n}) \\ \\ n & (n \geq \bar{n}) \end{cases} \tag{30}$$

where $A = 1/\pi \cosh^{-1}(b)$. These null locations can be translated to null locations on the unit circle by the formula

$$\psi_n = 2\pi u_n / N . \tag{31}$$

From ψ_n, the factored form of p(s) is formed. Multiplying the terms together gives a polynomial whose coefficients are the Taylor weights.

A 20-element linear Taylor distribution with $\bar{n} = 5$ and -20 dB sidelobes has the following values

$$u_n = \pm 0.55, \pm 1.00, \pm 1.89, \pm 3.22, \pm 5, \pm 6, \pm 7 \quad \pm 8, \pm 9, 10$$

$$A = 1.5 .$$

Converting u_n into ψ_n and forming the polynomial equation yields

$$\begin{aligned} p(s) = {} & 0.67s^{19} + 0.62s^{18} + 0.59s^{17} + 0.62s^{16} + 0.72s^{15} + 0.82s^{14} \\ & + 0.89s^{13} + 0.93s^{12} + 0.97s^{11} + s^{10} + s^{9} + 0.97s^{8} + 0.93s^{7} \\ & + 0.89s^{6} + 0.82s^{5} + 0.72s^{4} + 0.62s^{3} + 0.59s^{2} + 0.62s + 0.67 . \end{aligned} \tag{32}$$

Figure 7 shows the resultant far field pattern.

A difference pattern with low sidelobes requires a new set of weights. The amplitude distribution for sidelobes in a sum pattern will not result in the same low sidelobes in a difference pattern and vice versa. For instance, when the Taylor distribution derived above is used in the difference channel, the far field pattern in Figure 8 is obtained. In response to this problem, Bayliss developed a low sidelobe distribution similar to the Taylor distribution.[5] The Bayliss distribution is characterized by $\bar{n} - 1$ equally high sidelobes on either side of the mainbeam and the others decrease exponentially away from the mainbeam.

5. Bayliss, E. T. (1968) Design of monopulse antenna difference patterns with low sidelobes. The Bell System Technical Journal, May-June: 1968:623-650.

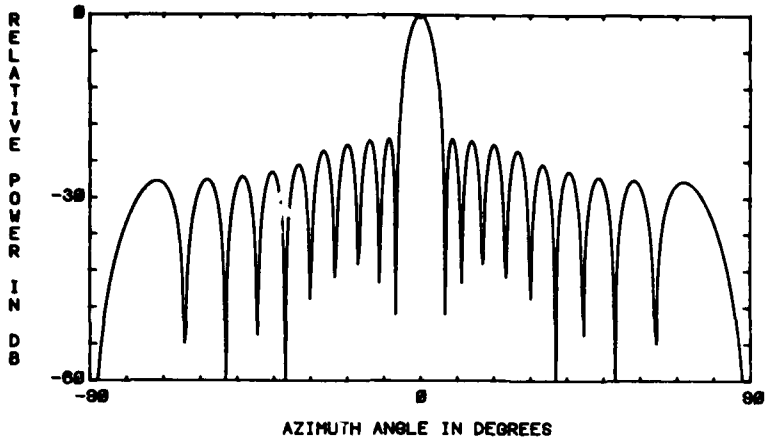

Figure 7. Far Field Pattern of a 20-Element Array With a 20 dB, $\bar{n} = 5$ Taylor Distribution

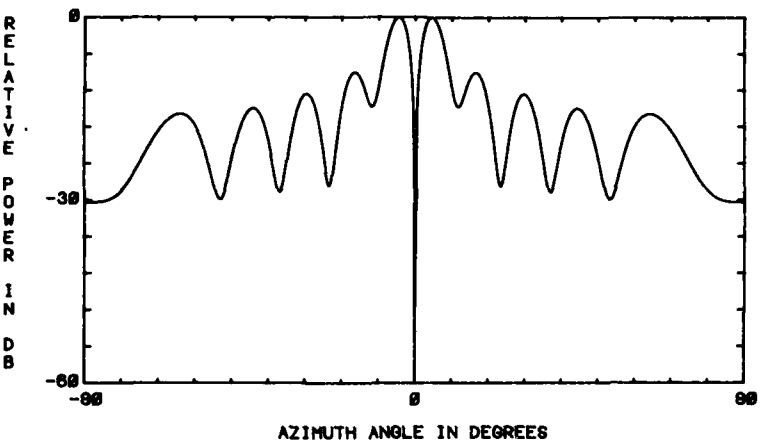

Figure 8. Far Field Difference Pattern of a 20-Element Array With a 20 dB, $\bar{n} = 5$ Taylor Distribution

Null locations for this distribution are at[1]

$$u_n = \begin{cases} 0 & (n = 0) \\ (\bar{n} + 0.5)\left[\dfrac{\delta}{A^2 + \bar{n}^2}\right]^{1/2} & (1 \leq n \leq 4) \\ (n + 0.5)\left[\dfrac{A^2 + n^2}{A^2 + \bar{n}^2}\right]^{1/2} & (5 \leq n \leq \bar{n} - 1) \\ n & (n \geq \bar{n}) \, . \end{cases} \tag{33}$$

The values for δ_n are given in Table 1. The variable A has the same value as it did for the Taylor distribution. ψ_n is found by using Eq. (31). Finally, the polynomial coefficients are found from ψ_n.

Table 1. Constants for Bayliss Distribution[1]

Bayliss Parameter	Sidelobe Level in dB					
	15	20	25	30	35	40
A	1.0079	1.2247	1.4355	1.6413	1.8431	2.0415
δ_1	1.5124	1.6962	1.8826	2.0708	2.2602	2.4504
δ_2	2.2561	2.3698	2.4943	2.6275	2.7675	2.9123
δ_3	3.1693	3.2473	3.3351	3.4314	3.5352	3.6452
δ_4	4.1264	4.1854	4.2527	4.3276	4.4093	4.4973

Consider a 20-element array with $\bar{n} = 5$ and -20 dB sidelobes. The values for u_n are

$$\pm 1.81, \pm 2.53, \pm 3.47, \pm 4.47, \pm 5, \pm 6, \pm 7, \pm 8, \pm 9, 10 \, .$$

In turn, the polynomial p(s) is found.

$$\begin{aligned} p(s) = {} & 0.65s^{19} + 0.71s^{18} + 0.82s^{17} + 93s^{16} + s^{15} + 0.99s^{14} \\ & + 0.90s^{13} + 0.72s^{12} + 0.46s^{11} + 0.16s^{10} - 0.16s^{9} \\ & - 0.46^{8} - 0.72s^{7} - 0.90s^{6} - 0.99s^{5} - s^{4} - 0.93s^{3} - 0.82s^{2} \\ & - 0.71s - 0.65 \end{aligned} \tag{34}$$

The coefficients of p(s) give the far field pattern shown in Figure 9.

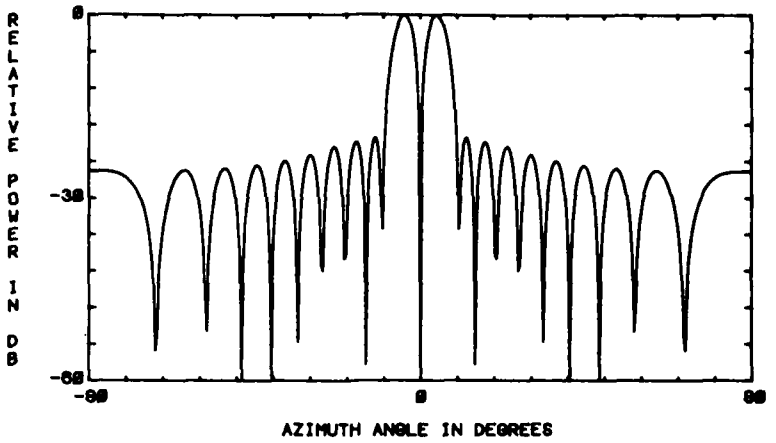

Figure 9. Far Field Difference Pattern of a 20-Element Array With a 20 dB, $\bar{n} = 5$ Bayliss Distribution

The remainder of this report describes several nulling techniques. The unit circle is a useful tool in understanding the nulling process. An antenna has only a fixed number of zeros on the unit circle (called degrees of freedom). In order to place a null in a desired direction, one of the degrees of freedom must be used. An N element array has N - 1 degrees of freedom. Thus, the amplitude weights for the 20-element Taylor and Bayliss arrays derived earlier have only 19 degrees of freedom.

3. AMPLITUDE AND PHASE NULLING

The nulling techniques described in the next two sections are based on the beam space algorithm described by Shore and Steyskal.[6] The algorithm is modified for difference patterns and for simultaneous nulling in sum and difference patterns. The algorithm is one that minimally perturbs the array weights (in a Least Mean Square sense) when forming the null. In this way, the amplitude and phase of the adaptive weights produce very little distortion to the quiescent far field pattern.

The algorithm described is a null synthesis technique rather than a closed loop adaptive algorithm. The location of the jammers must be known for the nulls to be placed. The phase and amplitude distribution that places nulls in the direction of the jammers while minimally perturbing the adaptive weights is then computed. The

6. Shore, R.A., and Steyskal, H. (1982) Nulling in Linear Array Patterns With Minimization of Weight Perturbations, RADC-TR-82-32, AD A118695.

weights used to generate this distribution theoretically yield a far field pattern with the desired nulls. In a practical situation, however, antenna errors significantly limit this nulling technique unless the weights are adaptively adjusted using some form of feedback. It is possible to convert this open loop null synthesis algorithm into a closed loop adaptive algorithm to compensate for the antenna errors. However, that practical implementation is outside the scope of this report.

3.1 Sum Channel

Figure 1 serves as the model for amplitude and phase nulling in both channels using separate weights for each channel. The quiescent weights for the sum channel are given by

$$w_{on} = a_n e^{-jd_n u_s} . \tag{35}$$

Assume that a weight change of Δw_n will produce the required nulls in the far field pattern. The new cascaded weights are represented by

$$w_n = w_{on}(1+ \Delta w_n) . \tag{36}$$

The weight change in complex form is

$$\Delta w_n = \alpha_n + j\beta_n . \tag{37}$$

When there are no weight changes, $\Delta w_n = 0$ and $w_n = w_{on}$. Substituting Eqs. (35) and (37) into Eq. (36) leads to

$$w_n = a_n e^{-jd_n u_s} (1 + \alpha_n + j\beta_n) . \tag{38}$$

This new amplitude and phase distribution puts nulls in the direction of the jammers.

The far field sum pattern of the adapted antenna is given by

$$S(u) = \sum_{n=1}^{N} a_n e^{-jd_n u_s} (1 + \alpha_n + j\beta_n) e^{jd_n u} \tag{39}$$

$$= \sum_{n=1}^{N} a_n e^{jd_n(u-u_s)} + \sum_{n=1}^{N} a_n(\alpha_n + j\beta_n) e^{jd_n(u-u_s)} \tag{40}$$

$$= S_o(u) + \sum_{n=1}^{N} a_n(\alpha_n + j\beta_n) e^{jd_n(u-u_s)} . \tag{41}$$

$$S_o(u) = \sum_{n=1}^{N} a_n \left\{ \cos [d_n(u - u_s)] + j \sin [d_n(u - u_s)] \right\} . \quad (42)$$

and, assuming $a_n = a_{N+1-n}$,

$$S_o(u) = \sum_{n=1}^{N} a_n \cos [d_n(u - u_s)] . \quad (43)$$

The sine terms sum to zero because d_n in Eq. (3a) is odd symmetric and the sine is an odd function. In general, M nulls are required in the pattern to cancel M jammers at angular locations u_m ($1 \leq m \leq M$). The resultant far field pattern equals zero when $u = u_m$.

$$S(u_m) + \sum_{n=1}^{N} a_n (\alpha_n + j\beta_n) e^{j d_n (u_m - u_s)} = 0 \quad (44)$$

for $m = 1, 2, \ldots, M$.

This system of equations may be looked at as the sum of the quiescent pattern and M cancellation beams. Each cancellation beam matches the quiescent pattern's amplitude in the jammer directions, but is opposite in phase. Therefore, the sum of the two quantities equals zero at u_m. The process is pictorially represented in Figure 10.

The above system of equations has M equations and N unknowns. To determine the values of Δw_n, Eq. (44) is solved for α_n and β_n. Shore and Steyskal have shown that minimizing the quantity $\sum_{n=1}^{N} (\alpha_n^2 + \beta_n^2)$ minimizes, in the least mean square sense, the adaptive weight perturbations. This is a very desirable characteristic, because the nulled pattern changes very little from its quiescent form.

To solve the system of equations, we put it into matrix form.

$$AX = B \quad (45)$$

where

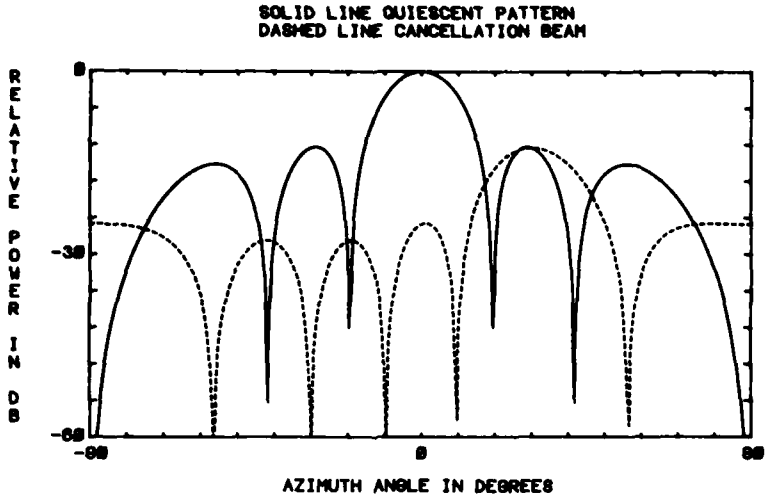

Figure 10. Cancellation Beam and Quiescent Pattern

$$A = \begin{bmatrix} a_1 e^{jd_1(u_1 u_s)} & a_2 e^{jd_2(u_1 - u_s)} & \cdots & a_N e^{jd_N(u_1 - u_s)} \\ a_1 e^{jd_1(u_2 - u_s)} & a_2 e^{jd_2(u_2 - u_s)} & \cdots & a_N e^{jd_N(u_2 - u_s)} \\ \vdots & \vdots & & \vdots \\ a_1 e^{jd_1(u_M - u_s)} & a_2 e^{jd_2(u_M - u_s)} & \cdots & a_N e^{jd_N(u_M - u_s)} \end{bmatrix} \quad (46)$$

$$X = [\alpha_1 + j\beta_1, \alpha_2 + j\beta_2, \ \ldots \alpha_N + j\beta_N]^T \quad (47)$$

$$B = -[S_o(u_1), S_o(u_2), \ \ldots \ S_o(u_M)]^T \quad (48)$$

where $[\ \ ]^T$ represents the transpose of a matrix.

The least squares solution[7] to AX = B is

$$A^\dagger AX = A^\dagger B \quad (49)$$

where $(\ \ )^\dagger$ represents the conjugate matrix transpose.

7. Derusso, P. M., Roy, R. J., and Close, C. M. (1965) State Variables for Engineers, John Wiley & Sons, Inc., New York.

$$(A^{\dagger}A)^{-1}\,(A^{\dagger}A)X = (A^{\dagger}A)^{-1}\,A^{\dagger}B \tag{50}$$

$$X = A^{\dagger}\,(AA^{\dagger})^{-1}\,B\,, \tag{51}$$

since it can be shown that $(A^{\dagger}A)^{-1}\,A^{\dagger} = A^{\dagger}\,(AA^{\dagger})^{-1}$.

The product of $AA^{\dagger}$ is a matrix whose elements are

$$(AA^{\dagger})_{km} = \sum_{n=1}^{N} a_n\, e^{jd_n(u_k - u_s)}\, a_n\, e^{jd_n(u_s - u_m)} \tag{52}$$

$$= \sum_{n=1}^{N} a_n^2\, e^{jd_n(u_k - u_m)} \tag{53}$$

$$= \sum_{n=1}^{N} a_n^2 \left\{\cos[d_n(u_k - u_m)] + j\sin[d_n(u_k - u_m)]\right\} \tag{54}$$

$$= \sum_{n=1}^{N} a_n^2 \cos[d_n(u_k - u_m)] \text{ for } k,\ m = 1,\ 2,\ \ldots,\ M\,. \tag{55}$$

The sine term sums to zero because d_n is odd symmetric, the sine is an odd function, and it has been assumed $a_n = a_{N+1-n}$.

Equation (51) may be written as

$$X = A^{\dagger}Y \tag{56a}$$

where

$$Y = (AA^{\dagger})^{-1}\,B\,. \tag{56b}$$

The vector Y is found by inverting $(AA^{\dagger})$ and post-multiplying the result by the vector B. Substituting Y into Eq. (51) gives

$$\alpha_n + j\beta_n = \sum_{m=1}^{M} y_m a_n \left\{\cos[d_n(u_s - u_m)] + j\sin[d_n(u_s - u_m)]\right\}\,. \tag{57}$$

Next, the real and imaginary parts are equated

$$\alpha_n = \sum_{m=1}^{M} y_m a_n \cos[d_n(u_s - u_m)] \tag{58}$$

$$\beta_n = \sum_{m=1}^{M} y_m a_n \sin[d_n(u_s - u_m)]\,. \tag{59}$$

The derived weight changes, $\Delta w_n = \alpha_n + j\beta_n$, are used to adjust the complex array weights to generate the nulls in the pattern. Using Eq. (36) the adapted weights may be expressed as

$$w_n = w_{on}\,\gamma_n \exp[j\phi_n]$$

where

$$\gamma_n = [(\alpha_n + 1)^2 + \beta_n^2]^{1/2} \tag{60}$$

$$\phi_n = \tan^{-1}[\beta_n/(\alpha_n + 1)]. \tag{61}$$

3.2 Difference Channel

The nulling technique can be extended to include difference patterns. Since the sum pattern is an even function and the difference pattern an odd function, the derivations require modification. Weight perturbations that create a desired null in the sum pattern do not create a null in the difference pattern, even if the amplitude distributions are uniform.

One way of producing a difference pattern is shown in Figure 1 where half of the element signals receive a 180° phase shift. The quiescent difference channel weights are

$$w_{on} = b_n e^{-jd_n u_s}. \tag{62}$$

As before, the weight change Δw_n produces a null in a desired direction.

$$w_n = w_{on}(1 + \Delta w_n) \tag{63}$$

$$= b_n e^{-jd_n u_s}(1 + \alpha_n + j\beta_n). \tag{64}$$

These weights have a far field pattern represented by

$$D(u) = \sum_{n=1}^{N} b_n e^{jd_n(u - u_s)} + \sum_{n=1}^{N} b_n e^{-jd_n u_s}(\alpha_n + j\beta_n) e^{jd_n u} \tag{65}$$

$$= D_o(u_m) + \sum_{n=1}^{N} b_n (\alpha_n + j\beta_n) e^{jd_n(u - u_s)}. \tag{66}$$

The quiescent far field pattern is

$$D_o(u) = \sum_{n=1}^{N} b_n \left\{ \cos[d_n(u - u_s)] + j \sin[d_n(u - u_s)] \right\} . \tag{67}$$

D(u) is zero in the direction of the jammers

$$\sum_{n=1}^{N} (\alpha_n + j\beta_n) b_n e^{jd_n(u_m - u_s)} = -D_o(u_m)$$

$$= - \sum_{n=1}^{N} \left\{ b_n \cos[d_n(u_m - u_s)] + j \sin[d_n(u_m - u_s)] \right\} . \tag{68}$$

Because b_n is an odd function

$$- \sum_{n=1}^{N} b_n \cos[d_n(u_m - u_s)] = 0 . \tag{69}$$

Equation (68) in matrix form is AX = B where

$$A = \begin{bmatrix} b_1 e^{jd_1(u_1 - u_s)} & b_2 e^{jd_2(u_1 - u_s)} & \cdots & b_N e^{jd_N(u_1 - u_s)} \\ b_1 e^{jd_1(u_2 - u_s)} & b_2 e^{jd_2(u_2 - u_s)} & \cdots & b_N e^{jd_N(u_2 - u_s)} \\ \vdots & \vdots & & \vdots \\ b_1 e^{jd_1(u_M - u_s)} & b_2 e^{jd_2(u_M - u_s)} & \cdots & b_N e^{jd_N(u_M - u_s)} \end{bmatrix} \tag{70a}$$

$$B = -[D_o(u_1), D_o(u_2), \ldots, D_o(u_M)]^T \tag{70b}$$

$$X = [\alpha_1 + j\beta_1, \alpha_2 + j\beta_2, \ldots \alpha_N + j\beta_N]^T . \tag{70c}$$

The method of least squares leads to a solution

$$X = A^\dagger (AA^\dagger)^{-1} B \tag{71a}$$

$$= A^\dagger C \tag{71b}$$

$$\alpha_n + j\beta_n = \sum_{m=1}^{M} c_m b_n e^{jd_n(u_m - u_s)} . \tag{72}$$

The variable c_m is an element of the vector C.

The matrix $(AA^\dagger)$ contains the elements

$$(AA^\dagger)_{km} = \sum_{n=1}^{N} b_n e^{jd_n(u_m - u_s)} b_n e^{-jd_n(u_k - u_s)} \tag{73}$$

$$= \sum_{n=1}^{N} b_n^2 e^{jd_n(u_m - u_k)} \tag{74}$$

$$= \sum_{n=1}^{N} b_n^2 \cos[d_n(u_m - u_k)] + j \sin[d_n(u_m - u_k)] . \tag{75}$$

The sine terms sum to zero leaving

$$(AA^\dagger)_{km} = \sum_{n=1}^{N} b_n^2 \cos[d_n(u_k - u_m)] . \tag{76}$$

Rewriting Eq. (72) results in

$$\alpha_n + j\beta_n = \sum_{m=1}^{M} c_m b_n \left\{ \cos[d_n(u_m - u_s)] + j \sin[d_n(u_m - u_s)] \right\} . \tag{77}$$

Finally, equating the real and imaginary parts of both sides of the equation produces the weight perturbations,

$$\alpha_n = \sum_{m=1}^{M} c_m b_n \cos[d_n(u_m - u_s)] \tag{78}$$

$$\beta_n = \sum_{m=1}^{M} c_m b_n \sin[d_n(u_m - u_s)] .$$

The phase-amplitude forms of the complex perturbations are used to adjust the variable complex weights.

3.3 Simultaneous Nulling in the Sum and Difference Channels

Null synthesis for sum and difference patterns in the manner previously described requires two separate sets of adaptive weights. Implementing this technique on a monopulse radar antenna requires N complex weights in the sum channel and N complex weights in the difference channel as shown in Figure 1. The following

pages describe a technique that allows the sum and difference channels to share one set of complex weights (Figure 11). The adaptive weight appears before the element signal is split into the sum and difference channels. Incorporating such a technique into an adaptive antenna would significantly reduce the cost and complexity of the system.

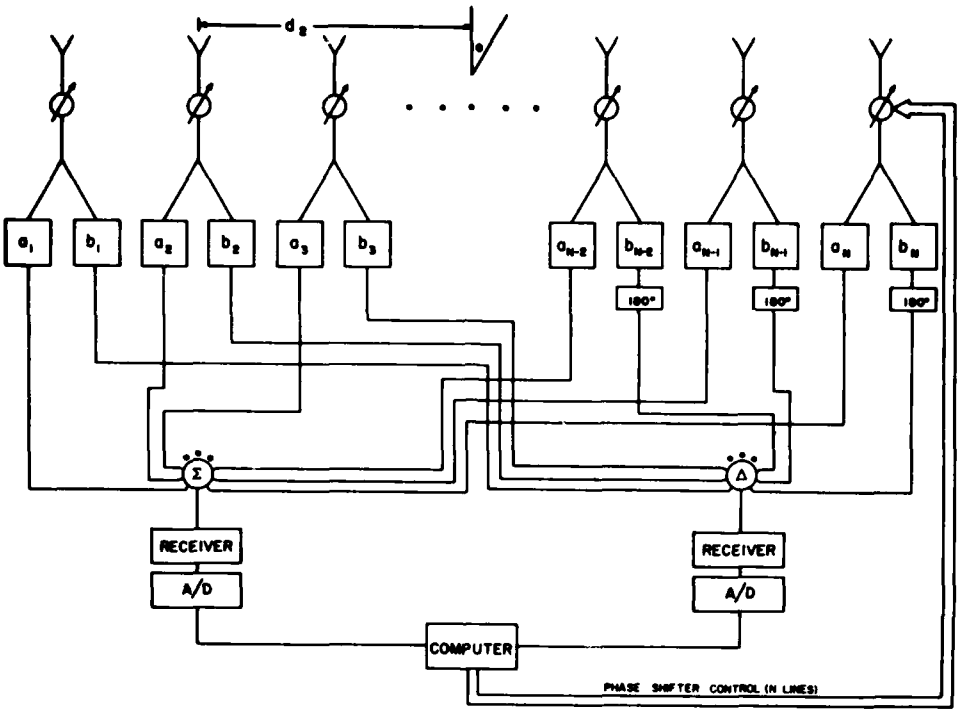

Figure 11. Monopulse Linear Array

A linear array with N elements has N complex weights and N-1 degrees of freedom. For every jammer, the sum channel uses one degree of freedom and the difference channel another. The drawback to this technique is that the degrees of freedom available for nulling in the sum and difference channels are cut in half, so that (N-1)/2 degrees of freedom are available.

Equations (44) and (68) still hold true, but now they must be solved simultaneously.

$$\sum_{n=1}^{N} (\alpha_n + j\beta_n)\, a_n\, e^{jd_n(u_m - u_s)} = \sum_{n=1}^{N} a_n \cos[(u_m - u_s)] \tag{80}$$

$$\sum_{n=1}^{N} (\alpha_n + j\beta_n)\, b_n\, e^{jd_n(u_m - u_s)} = -j \sum_{n=1}^{N} b_n \sin[(d_n(u_m - u_s)]\,. \tag{81}$$

This system of equations may be put in the form AX = B

$$A = \begin{bmatrix} a_1 e^{jd_1(u_1 - u_s)} & \cdots & a_N e^{jd_N(u_1 - u_s)} \\ \vdots & & \vdots \\ a_1 e^{jd_1(u_M - u_s)} & \cdots & a_N e^{jd_N(u_M - u_s)} \\ b_1 e^{jd_i(u_1 - u_s)} & \cdots & b_N e^{jd_N(u_1 - u_s)} \\ \vdots & & \vdots \\ b_1 e^{jd_1(u_M - u_s)} & \cdots & b_N e^{jd_N(u_M - u_s)} \end{bmatrix} \tag{82}$$

$$X = \begin{bmatrix} \alpha_1 + j\beta_1 \\ \alpha_2 + j\beta_2 \\ \vdots \\ \alpha_N + j\beta_N \end{bmatrix} \tag{83}$$

$$B = \begin{bmatrix} -\sum_{n=1}^{N} a_n \cos[d_n(u_1 - u_s)] \\ \vdots \\ -\sum_{n=1}^{N} a_n \cos[d_n(u_M - u_s)] \\ -j\sum_{n=1}^{N} b_n \sin[d_n(u_1 - u_s)] \\ \vdots \\ -j\sum_{n=1}^{N} b_n \sin[d_n(u_M - u_s)] \end{bmatrix} \tag{84}$$

The least mean square solution to the equation is

$$X = A^{\dagger}(AA^{\dagger})\,B\,. \tag{85}$$

To make the computations easier to follow, the A matrix is partitioned.

$$A = \begin{bmatrix} J \\ K \end{bmatrix} \tag{86}$$

$$(AA^{\dagger}) = \begin{bmatrix} J \\ K \end{bmatrix} \begin{bmatrix} J^{*} & K^{*} \end{bmatrix}^{\dagger} \tag{87}$$

$$= \begin{bmatrix} JJ^{*} & JK^{*} \\ KJ^{*} & KK^{*} \end{bmatrix}\,. \tag{88}$$

The elements for $(AA^{\dagger})$ are

$$(AA^{\dagger})_{j,k} = \sum_{n} a_n^2\, e^{jd_n(u_j - u_k)} \tag{89}$$

$$(AA^{\dagger})_{j+M,k} = \sum_{n} a_n\, b_n\, e^{jd_n(u_j - u_k)} \tag{90}$$

$$(AA^{\dagger})_{j,k+M} = \sum_{n} a_n\, b_n\, e^{jd_n(u_j - u_k)} \tag{91}$$

$$(AA^{\dagger})_{j+M,k+M} = \sum_{n} b_n^2\, e^{jd_n(u_j - u_k)}\,. \tag{92}$$

Inverting the complex matrix $(AA^{\dagger})$ and multiplying it by Y results in a 2M x 1 complex matrix R. The weight perturbations are

$$\alpha_n + j\beta_n = A^{\dagger}R \tag{93}$$

$$= \begin{bmatrix} a_1 e^{-jd_1(u_1 - u_s)} & \cdots & a_1 e^{-jd_1(u_M - u_s)} & b_1 e^{-jd_1(u_1 - u_s)} & \cdots & b_1 e^{-jd_1(u_M - u_s)} \\ \vdots & & \vdots & \vdots & & \vdots \\ a_N e^{-jd_N(u_1 - u_s)} & \cdots & a_N e^{-jd_N(u_M - u_s)} & b_N e^{-jd_N(u_1 - u_s)} & \cdots & b_N e^{-jd_N(u_M - u_s)} \end{bmatrix} \begin{bmatrix} f_1 + jg_1 \\ \vdots \\ f_{2M} + jg_{2M} \end{bmatrix} \tag{94}$$

$$= \sum_{m=1}^{M} (a_n f_m e^{-jd_n(u_m - u_s)} + ja_n g_m e^{-jd_n(u_m - u_s)} + b_n f_{m+M} e^{-jd_n(u_m - u_s)}$$

$$+ jb_n g_{m+M} e^{-jd_n(u_m - u_s)}) \quad (95)$$

$$\alpha_n = \sum_{m=1}^{M} \{a_n f_m \cos[d_n(u_m - u_s)] + a_n g_m \sin[d_n(u_m - u_s)]$$

$$+ b_n f_{m+M} \cos[d_n(u_m - u_s)] + b_n g_{m+M} \sin[d_n(u_m - u_s)]\} \quad (96)$$

$$\beta_n = \sum_{m=1}^{M} \{-a_n f_m \sin[d_n(u_m - u_s)] + a_n g_m \cos[d_n(u_m - u_s)]$$

$$- b_n f_{m+M} \sin[d_n(u_m - u_s)] + b_n g_{m+M} \cos[d_n(u_m - u_s)]\} . \quad (97)$$

All three techniques were modeled on the computer and the results are shown in Section 5.

4. PHASE-ONLY NULLING

Nulling with phase shifters is much more desirable than nulling with complex weights. The hardware for phase-only nulling is less complicated. Adjusting the signal amplitude requires an attenuator or two phase shifters in a bridge circuit for each element. The extra losses, mismatch, and cost of the amplitude control discourages its use. Also, phased arrays usually have only phase shifters and incorporation of amplitude weighting requires modifications to existing antennas. An adaptive technique that uses phase control rather than phase and amplitude control can more easily be implemented on existing phased arrays.

4.1 Sum Channel

Phase only nulling in the sum channel of a low sidelobe antenna is discussed in the literature.[8] The technique closely follows the process used in phase and amplitude nulling. The quiescent sum channel weights are given by Eq. (35). To put nulls in the antenna pattern, a phase shift of ϕ_n is given to each element.

8. Baird, C.A., and Rassweiler, G.C. (1976) Adaptive nulling using digitally controlled phase-shifters, IEE Trans. on Antennas and Propagation, 24(No. 5):638-649.

$$w_n = a_n e^{-jd_n u_s} e^{j\phi_n} \tag{98}$$

$$\simeq a_n e^{-jd_n u_s}(1 + j\phi_n),\ \phi_n << 1\ . \tag{99}$$

The approximation $e^{j\phi_n} \simeq 1 + j\phi_n$ is necessary to solve the problem, but it makes the answer approximate. Fortunately, this approximation works very well for low sidelobe antennas.[8]

The far field pattern of these weights is calculated from

$$S(u) = \sum_{n=1}^{N} a_n e^{-jd_n u_s}(1 + j\phi_n) e^{jd_n u} \tag{100}$$

$$= \sum_{n=1}^{N} a_n e^{jd_n(u - u_s)} + j \sum_{n=1}^{N} a_n \phi_n e^{jd_n(u - u_s)}\ . \tag{101}$$

At the jammer angles, the pattern goes to zero

$$S(u_m) = \sum_{n=1}^{N} a_n e^{jd_n(u_m - u_s)} + j \sum_{n=1}^{N} a_n \phi_n e^{jd_n(u_m - u_s)} = 0 \tag{102}$$

$$j \sum_{n=1}^{N} a_n \phi_n \left\{ \cos[d_n(u_m - u_s)] + j \sin[d_n(u_m - u_s)] \right\}$$

$$= - \sum_{n=1}^{N} a_n \left\{ \cos[d_n(u_m - u_s)] + j \sin[d_n(u_m - u_s)] \right\}\ . \tag{103}$$

Next, equating the real and imaginary parts, assuming a_n real

$$\sum_{n=1}^{N} a_n \phi_n \sin[d_n(u_m - u_s)] = \sum_{n=1}^{N} a_n \cos[d_n(u_m - u_s)] \tag{104}$$

$$\sum_{n=1}^{N} a_n \phi_n \cos[d_n(u_m - u_s)] = \sum_{n=1}^{N} a_n \sin[d_n(u_m - u_s)]\ . \tag{105}$$

The second equation equals zero because the sine is an odd function, d_n has odd symmetry, and $a_{N+1} = a_n$ has been assumed.

Equation (104) can be put into the matrix form $AX = B$ where

$$A = \begin{bmatrix} a_1 \sin[d_1(u_1 - u_s)] & \cdots & a_N \sin[d_N(u_1 - u_s)] \\ \vdots & & \vdots \\ a_1 \sin[d_1(u_M - u_s)] & \cdots & a_N \sin[d_N(u_M - u_s)] \end{bmatrix} \tag{106}$$

$$X = \begin{bmatrix} \phi_1 \\ \phi_2 \\ \vdots \\ \phi_N \end{bmatrix}$$

$$B = \begin{bmatrix} \sum_{n=1}^{N} a_n \cos[d_n(u_1 - u_s)] \\ \vdots \\ \sum_{n=1}^{N} a_n \cos[d_n(u_M - u_s)] \end{bmatrix}$$

The unknown phase shifts are obtained from the method of least squares.

$$X = A^T C \tag{109}$$

$$C = (AA^T)^{-1} B \tag{110}$$

$$(AA^T)_{jk} = \sum_n a_n^2 \sin[(d_n(u_j - u_s)] \sin[d_n(u_k - u_s)] \tag{111}$$

$$\phi_n = \sum_{m=1}^{M} c_m a_n \sin[(d_n(u_m - u_s)] \, . \tag{112}$$

The variable c_m is the mth element in the vector C. Nulls are made in the sum pattern in the directions of the jammers when ϕ_n is applied to the phase shifters.

4.2 Difference Channel

The derivation of the phase shifts for the difference channel follows that of the sum channel.

$$\begin{aligned} w_n &= b_n e^{-j d_n u_s} e^{j\phi_n} \\ &\simeq b_n e^{-j d_n u_s} (1 + j\phi_n) \, . \end{aligned} \tag{113}$$

The far field difference pattern is

$$D(u) = \sum_{n=1}^{N} b_n (1 + j\varphi_n)\, e^{j d_n (u - u_s)} . \tag{114}$$

D(u) equals zero when $u = u_m$.

$$j \sum_{n=1}^{N} b_n \varphi_n \left\{ \cos[d_n(u_m - u_s)] + j \sin[d_n(u_m - u_s)] \right\}$$

$$= - \sum_{n=1}^{N} b_n \left\{ \cos[d_n(u_m - u_s)] + j \sin[d_n(u_m - u_s)] \right\} . \tag{115}$$

Equating the real and imaginary parts of the equation,

$$\sum_{n=1}^{N} b_n \varphi_n \cos[d_n(u_m - u_s)] = - \sum_{n=1}^{N} b_n \sin[d_n(u_m - u_s)] \tag{116}$$

$$= \sum_{n=1}^{N} b_n \varphi_n \sin[d_n(u_m - u_s)] = - \sum_{n=1}^{N} b_n \cos[d_n(u_m - u_s)] . \tag{117}$$

Equation (116) equals zero.

The remaining system of equations can be solved using the method of least squares.

$$AX = B \tag{118}$$

$$X = A^T (AA^T)^{-1} B \tag{119a}$$

$$= A^T C \tag{119b}$$

$$A = \begin{bmatrix} b_1 \cos[d_1(u_1 - u_s)] & \cdots & b_N \cos[d_N(u_1 - u_s)] \\ \vdots & & \vdots \\ b_1 \cos[d_1(u_M - u_s)] & \cdots & b_N \cos[d_N(u_M - u_s)] \end{bmatrix} \tag{120}$$

$$B = \begin{bmatrix} - \sum_{n=1}^{N} b_n \sin[d_n(u_1 - u_s)] \\ \vdots \\ - \sum_{n=1}^{N} b_n \sin[d_n(u_M - u_s)] \end{bmatrix} . \tag{121}$$

The X vector contains the values ϕ_n and C has elements c_m.

$$\phi_n = \sum_{m=1}^{M} c_m b_n \cos[d_n(u_m - u_s)] .$$

These phase shifts produce nulls in the difference pattern in the directions of interference.

4.3 Simultaneous Nulling in the Sum and Difference Channels

Normally, both the sum and difference channels share one set of phase shifters. The preceding nulling techniques place nulls in the sum pattern or the difference pattern, but not both. To place the nulls in both far field patterns, the conditions of the two equations must be met. Thus, Eqs. (103) and (115) remain unchanged, but in this case, they are solved simultaneously.

The elements of the matrix equation AX = B are

$$A = \begin{bmatrix} a_1 \sin[d_1(u_1 - u_s)] & \cdots & a_N \sin[d_N(u_1 - u_s)] \\ \vdots & & \vdots \\ a_1 \sin[d_1(u_M - u_s)] & \cdots & a_N \sin[d_N(u_M - u_s)] \\ b_1 \cos[d_1(u_1 - u_s)] & \cdots & b_N \cos[d_N(u_1 - u_s)] \\ \vdots & & \vdots \\ b_1 \cos[d_1(u_M - u_s)] & \cdots & b_N \cos[d_N(u_M - u_s)] \end{bmatrix} \qquad (123)$$

$$X = \begin{bmatrix} \phi_1 \\ \phi_2 \\ \vdots \\ \phi_N \end{bmatrix} \qquad (124)$$

$$B = \begin{bmatrix} \sum_{n=1}^{N} a_n \cos[d_n(u_1 - u_s)] \\ \vdots \\ \sum_{n=1}^{N} a_n \cos[d_n(u_M - u_s)] \\ -\sum_{n=1}^{N} b_n \sin[d_n(u_1 - u_s)] \\ \vdots \\ -\sum_{n=1}^{N} b_n \sin[d_n(u_M - u_s)] \end{bmatrix} \tag{125}$$

The least squares solution is

$$X = A^T C \tag{126}$$

$$C = (AA^T)^{-1} B \tag{127}$$

$$(AA^T)_{i,j} = \sum_{n=1}^{N} a_n^2 \sin[d_n(u_i - u_s)] \sin[d_n(u_j - u_s)], \quad i, j \leq M \tag{128}$$

$$(AA^T)_{i+M,j} = \sum_{n=1}^{N} a_n b_n \sin[d_n(u_i - u_s)] \cos[d_n(u_j - u_s)] \tag{129}$$

$$(AA^T)_{i,j+N} = \sum_{n=1}^{N} a_n b_n \cos[d_n(u_i - u_s)] \sin[d_n(u_j - u_s)] \tag{130}$$

$$(AA^T)_{i+M,j+M} = \sum_{n=1}^{N} b_n^2 \cos[d_n(u_i - u_s)] \cos[d_n(u_j - u_s)] \tag{131}$$

$$\phi_n = \sum_{m=1}^{M} c_m a_n \sin[d_n(u_m - u_s)] \sum_{m=M+1}^{2M} c_m b_n \cos[d_n(u_m - u_s)] . \tag{132}$$

The variables c_m are elements of the matrix C. These values of ϕ_n simultaneously generate a null in the sum and difference patterns in the direction of interference.

5. SIMULATION RESULTS

I modeled the nulling techniques described in Sections 2 through 4 on the computer. Appendix A contains a block diagram and description of the program. This section shows the results of several computer runs of the model. The nulling results from this section are displayed in Table 2.

The antenna array was modeled after Figure 11. Both the sum and difference channels share one set of adaptive weights. The output for the channel is obtained by multiplying the received signal at each element by the adapted weight. Next, a 3 dB coupler sends half the signal to the sum channel and half to the difference channel. Each sum channel signal is multiplied by an amplitude weight then summed to obtain one output. The difference signal is obtained in a similar manner, except that half of the signals are phase shifted by 180° before being summed.

The first series of runs used a 10-element uniformly weighted linear array. Figures 12a and 12b show the quiescent far field sum and difference patterns and weights for the array. Initially, the adaptive amplitude and phase weights were set to 1.0. When a jammer was placed at 33°, these weights changed to produce a null in the pattern in that direction. If a null is placed only in the sum channel, the results in Figures 13a-13d are obtained. The sum channel weights in Figure 13a are obtained by multiplying the adapted weights by the sum channel amplitude distribution.

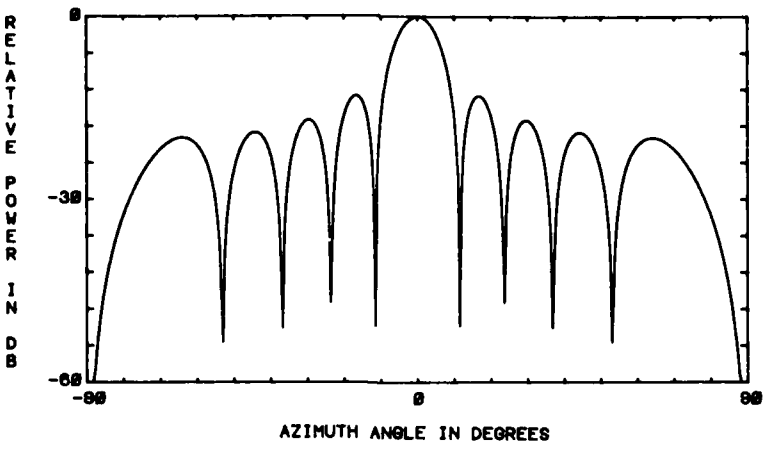

Figure 12a. Quiescent Far Field Sum-Channel Pattern of a 10-Element Uniform Array

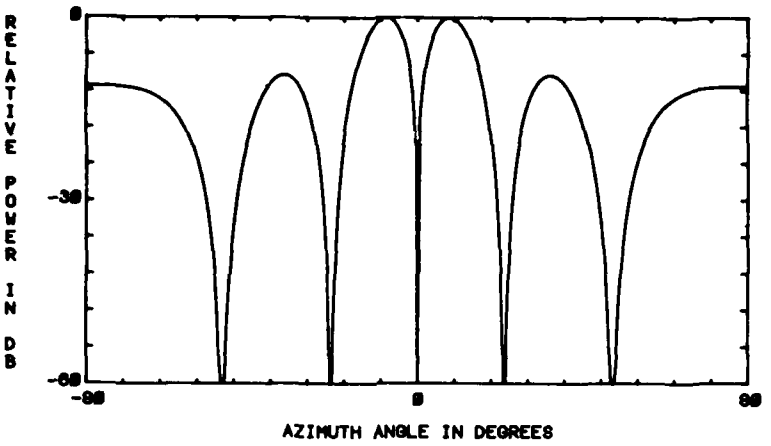

Figure 12b. Quiescent Far Field Difference-Channel Pattern of a 10-Element Uniform Array

	VARIABLE COMPLEX WEIGHTS		AMPLITUDE TAPERS	
ELEMENT	AMPLITUDE	PHASE	SUM CHAN	DIF CHANNEL
1	1.00000	0.00000	1.00000	−1.00000
2	1.00000	0.00000	1.00000	−1.00000
3	1.00000	0.00000	1.00000	−1.00000
4	1.00000	0.00000	1.00000	−1.00000
5	1.00000	0.00000	1.00000	−1.00000
6	1.00000	0.00000	1.00000	1.00000
7	1.00000	0.00000	1.00000	1.00000
8	1.00000	0.00000	1.00000	1.00000
9	1.00000	0.00000	1.00000	1.00000
10	1.00000	0.00000	1.00000	1.00000

Figure 12c. Quiescent Uniform Sum and Difference Channel Weights

The difference channel weights are the result of multiplying the adapted amplitude weights by the difference channel amplitude distribution. Adapted phase values are the same for both channels. Corresponding to the new adapted weights is the far field sum pattern shown in Figure 13b. Its quiescent pattern and associated cancellation beam are shown in Figure 13c. These same adapted weights do not yield a null in the difference pattern at 33° (Figure 13d).

Table 2. Nulling Results for Figures 12 to 26

FAR FIELD PATTERN AMPLITUDE (in DB below mainbeam)								
			Type of Nulling					
Aperture Distribution	Jammer Locations	Quiescent	A & P Sum	A & P Difference	A & P Simultaneous	PO Sum	PO Difference	PO Simultaneous
Uniform Sum	33°	20	240	20	258	69	19	63
Uniform Difference	33°	11	11	264	250	11	56	54
Taylor Sum	23°	46	249	46	167	115	46	87
	59°	38	253	38	243	84	38	81
Bayliss Difference	23°	42	42	256	161	42	100	76
	59°	50	50	263	159	48	90	89

A & P	- amplitude and phase nulling
PO	- phase only nulling
Sum	- nulling done in sum channel
Difference	- nulling done in difference channel
Simultaneous	- nulling done simultaneously in both channels

	VARIABLE COMPLEX WEIGHTS		VARIABLE WEIGHTS TIMES AMPLITUDE TAPERS	
ELEMENT	AMPLITUDE	PHASE	SUM CHAN	DIF CHANNEL
1	0.98951	−0.10124	0.98951	−0.98951
2	0.90362	0.03252	0.90362	−0.90362
3	1.04667	0.08782	1.04667	−1.04667
4	1.08633	−0.05069	1.08633	−1.08633
5	0.93674	−0.08166	0.93674	−0.93674
6	0.93674	0.08166	0.93674	0.93674
7	1.08633	0.05069	1.08633	1.08633
8	1.04667	−0.08782	1.04667	1.04667
9	0.90362	−0.03252	0.90362	0.90362
10	0.98951	0.10124	0.98951	0.98951

Figure 13a. Adapted Weights From Amplitude and Phase Nulling in the Sum Channel

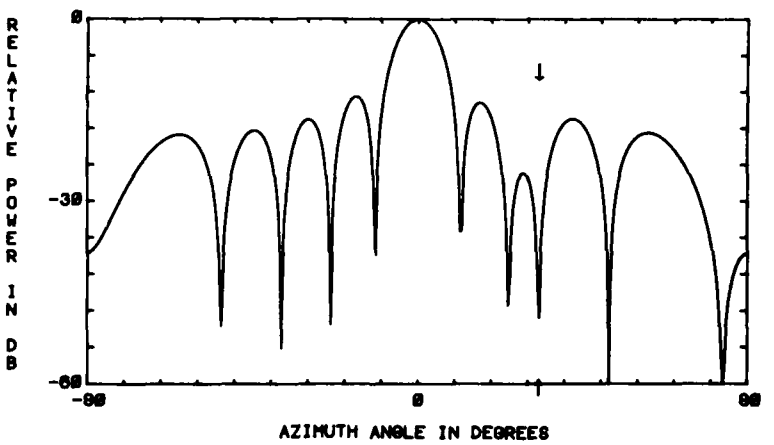

Figure 13b. Far Field Sum Pattern Due to Amplitude and Phase Nulling in the Sum Channel

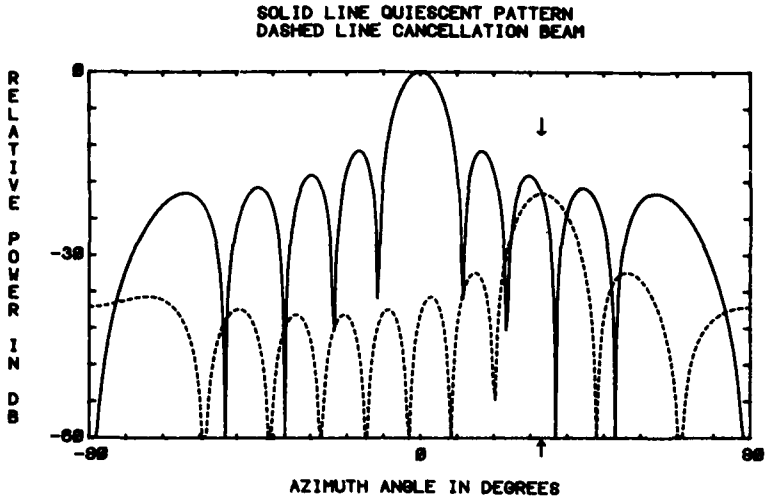

Figure 13c. Cancellation Beam From Amplitude and Phase Nulling in the Sum Channel

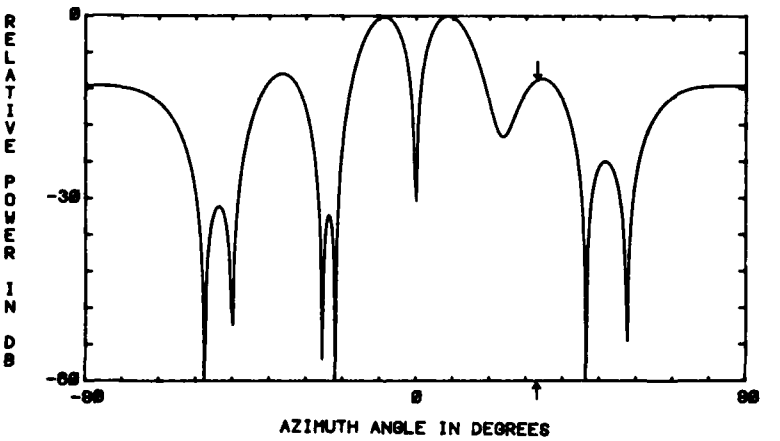

Figure 13d. Far Field Difference Pattern Due to Amplitude and Phase Nulling in the Sum Channel

Figures 14a-14d show the results of placing a null in the difference pattern at 33°. The new amplitude and phase distributions are different from those in Figure 4. They produce a null in the difference pattern at 33°, but not in the sum pattern.

	VARIABLE COMPLEX WEIGHTS		VARIABLE WEIGHTS TIMES AMPLITUDE TAPERS	
ELEMENT	AMPLITUDE	PHASE	SUM CHAN	DIF CHANNEL
1	0.78538	0.04267	0.78538	−0.78538
2	1.08353	0.19367	1.08353	−1.08353
3	1.20116	−0.07650	1.20116	−1.20116
4	0.90025	−0.20456	0.90025	−0.90025
5	0.84762	0.16942	0.84762	−0.84762
6	0.84762	−0.16942	0.84762	0.84762
7	0.90025	0.20456	0.90025	0.90025
8	1.20116	0.07650	1.20116	1.20116
9	1.08353	−0.19367	1.08353	1.08353
10	0.78538	−0.04267	0.78538	0.78538

Figure 14a. Adapted Weights From Amplitude and Phase Nulling in the Difference Channel

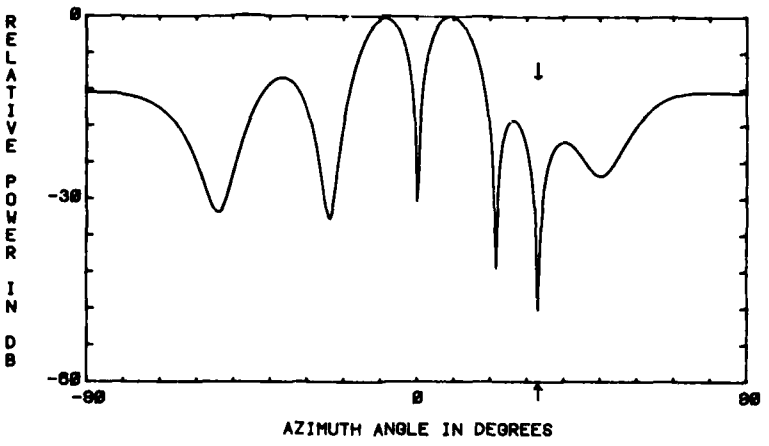

Figure 14b. Far Field Difference Pattern Due to Amplitude and Phase Nulling in the Difference Channel

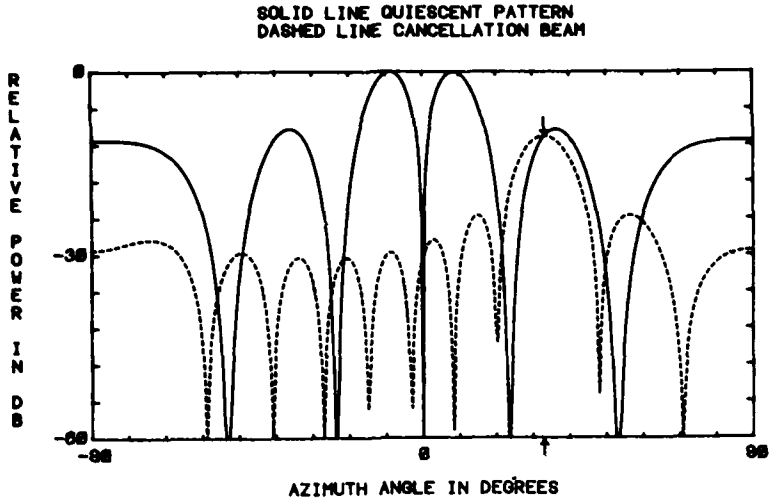

Figure 14c. Cancellation Beam From Amplitude and Phase Nulling in the Difference Channel

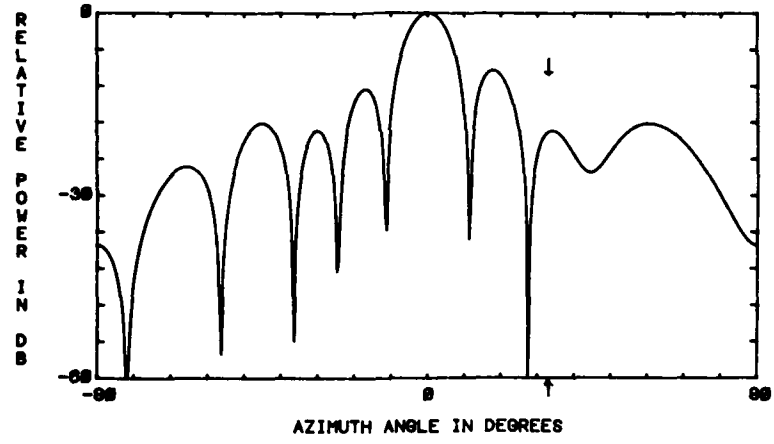

Figure 14d. Far Field Sum Pattern Due to Amplitude and Phase Nulling in the Difference Channel

These computer outputs demonstrate the need for simultaneous nulling in the sum and difference channels. Placing a null in one channel does not guarantee that the same null will appear in the other channel. When the simultaneous nulling algorithm was tried, the results in Figures 15a-15e were obtained. Both antenna patterns have nulls at 33°.

	VARIABLE COMPLEX WEIGHTS		VARIABLE WEIGHTS TIMES AMPLITUDE TAPERS	
ELEMENT	AMPLITUDE	PHASE	SUM CHAN	DIF CHANNEL
1	0.77198	–0.08627	0.77198	–0.77198
2	0.99527	0.24139	0.99527	–0.99527
3	1.24028	0.00000	1.24028	–1.24028
4	0.99527	–0.24139	0.99527	–0.99527
5	0.77198	0.08627	0.77198	–0.77198
6	0.77198	–0.08627	0.77198	0.77198
7	0.99527	0.24139	0.99527	0.99527
8	1.24028	0.00000	1.24028	1.24028
9	0.99527	–0.24139	0.99527	0.99527
10	0.77198	0.08627	0.77188	0.77198

Figure 15a. Adapted Weights From Amplitude and Phase Nulling in the Sum and Difference Channels Simultaneously

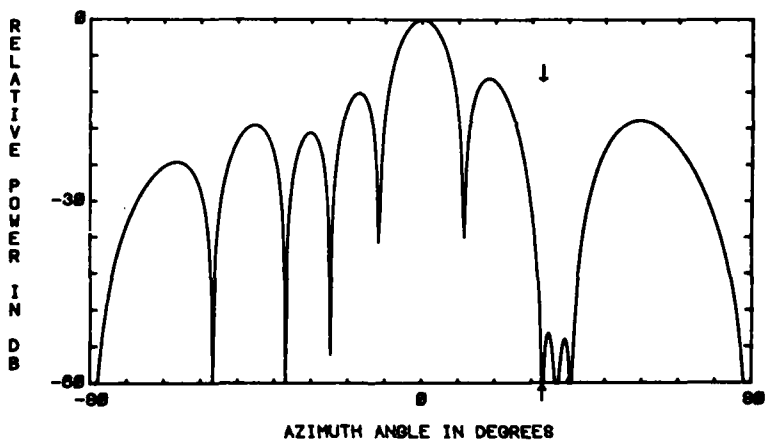

Figure 15b. Far Field Sum Pattern Due to Amplitude and Phase Nulling in the Sum and Difference Channels Simultaneously

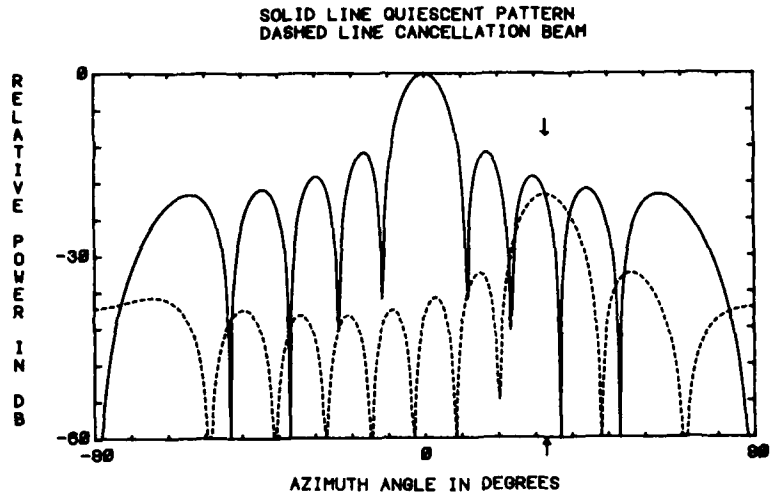

Figure 15c. Sum Channel Cancellation Beam From Amplitude and Phase Nulling in the Sum and Difference Channels Simultaneously

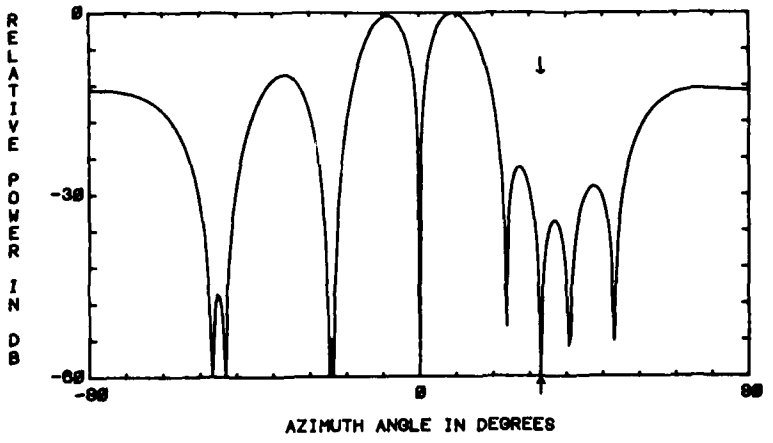

Figure 15d. Far Field Difference Pattern Due to Amplitude and Phase Nulling in the Sum and Difference Channels Simultaneously

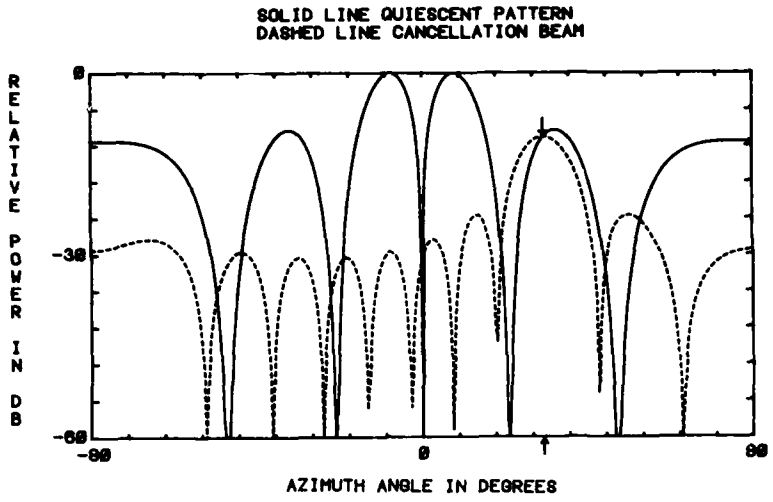

Figure 15e. Difference Channel Cancellation Beam From Amplitude and Phase Nulling in the Sum and Difference Channels Simultaneously

The case of one jammer at 33° was repeated for phase-only nulling. Figures 16a-16d are the results of nulling in the sum channel. No null appears in the difference pattern at 33°. Figures 17a-17d show the results of difference channel nulling. Again, the sum pattern does not have a null at 33°. When simultaneous nulling is used, both patterns have a null at 33° (Figures 18a-18e).

Note that the cancellation beams in the phase-only nulling cases have two main lobes: one at 33° and a replica at -33°. When added to the quiescent pattern, a null is produced at 33°, but the sidelobe level at -33° goes up. The cancellation lobe at 33° is out of phase with the quiescent pattern at 33°, while the lobe at -33° is in phase with the quiescent pattern at -33°. These separate beams may be mathematically derived by substituting Eq. (112) into Eq. (101). The cancellation beams are given by

$$C\ BEAMS = j \sum_{n=1}^{N} a_n e^{j d_n (u - u_s)} \sum_{m=1}^{M} c_m a_n \sin[d_n (u_m - u_s)] \tag{133}$$

$$= j \sum_{n=1}^{N} a_n e^{j d_n (u_m - u_s)} \sum_{m=1}^{M} c_m a_n \left[e^{j d_n (u_m - u_s)} - e^{j d_n (u_m - u_s)} / 2j \right] \tag{134}$$

This form of the equation reveals the two cancellation beams. They have the same amplitude, but conjugate angles and phases.

ELEMENT	PHASE SHIFT
1	–0.18191
2	0.05345
3	0.16697
4	–0.10013
5	–0.13898
6	0.13898
7	0.10013
8	–0.16697
9	–0.05345
10	0.18191

Figure 16a. Adapted Weights From Phase-Only Nulling in the Sum Channel

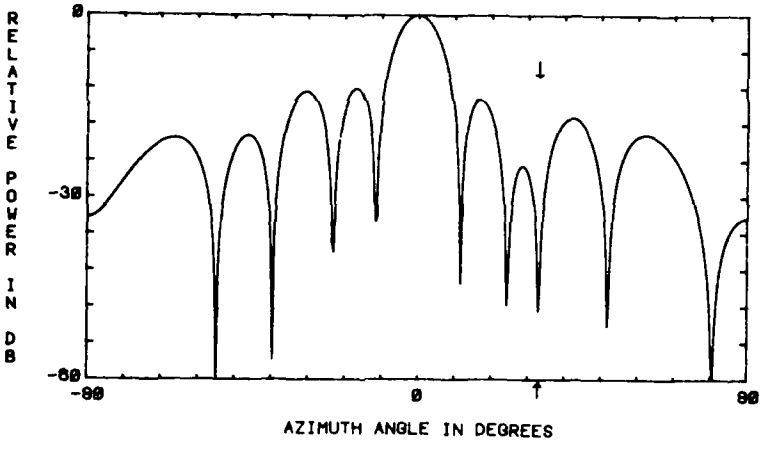

Figure 16b. Far Field Sum Pattern Due to Phase-Only Nulling in the Sum Channel

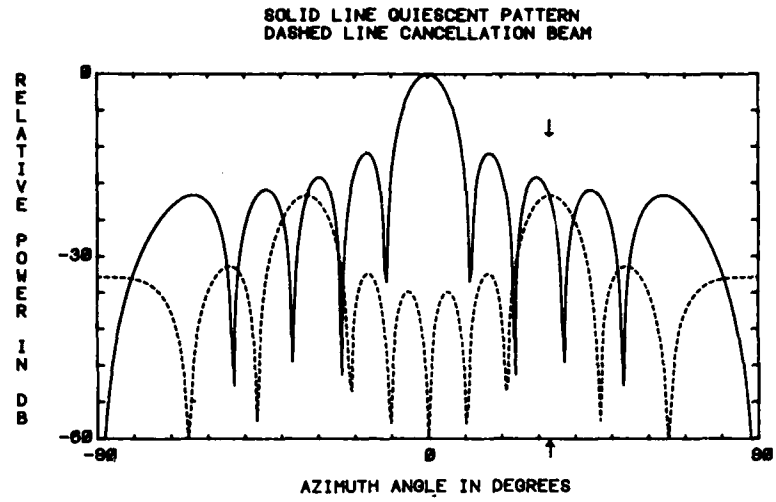

Figure 16c. Cancellation Beam From Phase-Only Nulling in the Sum Channel

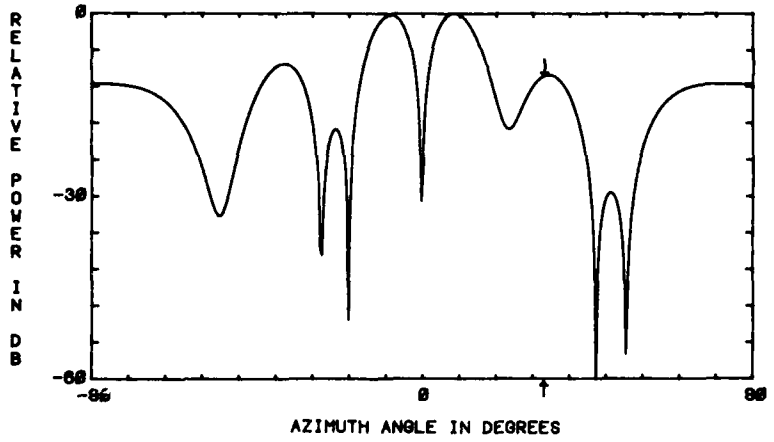

Figure 16d. Far Field Difference Pattern Due to Phase-Only Nulling in the Sum Channel

ELEMENT	PHASE SHIFT
1	0.07440
2	0.46319
3	–0.20389
4	–0.40619
5	0.31745
6	–0.31745
7	0.40619
8	0.20389
9	–0.46319
10	–0.07440

Figure 17a. Adapted Weights From Phase-Only Nulling in the Sum Channel

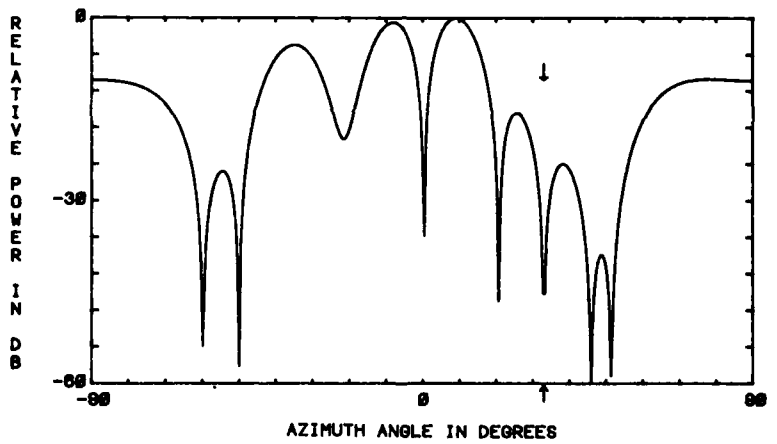

Figure 17b. Far Field Difference Pattern Due to Phase-Only Nulling in the Difference Channel

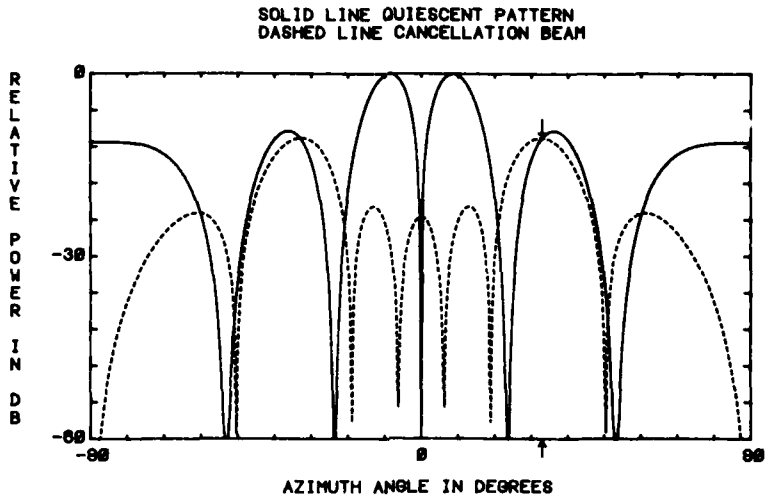

Figure 17c. Cancellation Beam From Phase-Only Nulling in the Difference Channel

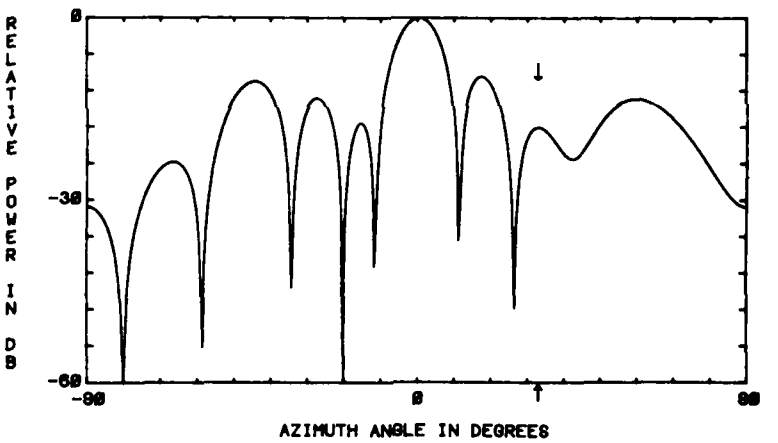

Figure 17d. Far Field Sum Pattern Due to Phase-Only Nulling in the Difference Channel

ELEMENT	PHASE SHIFT
1	–0.15730
2	0.56268
3	0.00000
4	–0.56268
5	0.15730
6	–0.15730
7	0.56268
8	0.00000
9	–0.56268
10	0.15730

Figure 18a. New Weights Obtained From Simultaneous Sum and Difference Channel Phase-Only Nulling

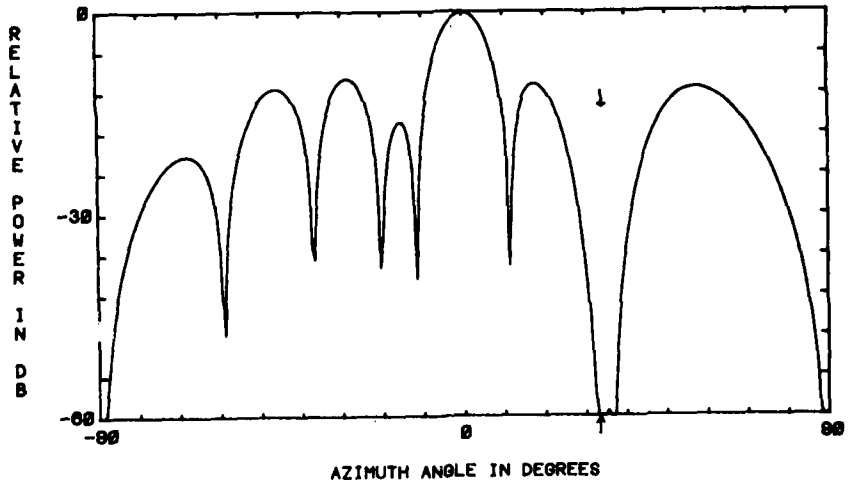

Figure 18b. Far Field Sum Pattern Due to Simultaneous Sum and Difference Channel Phase-Only Nulling

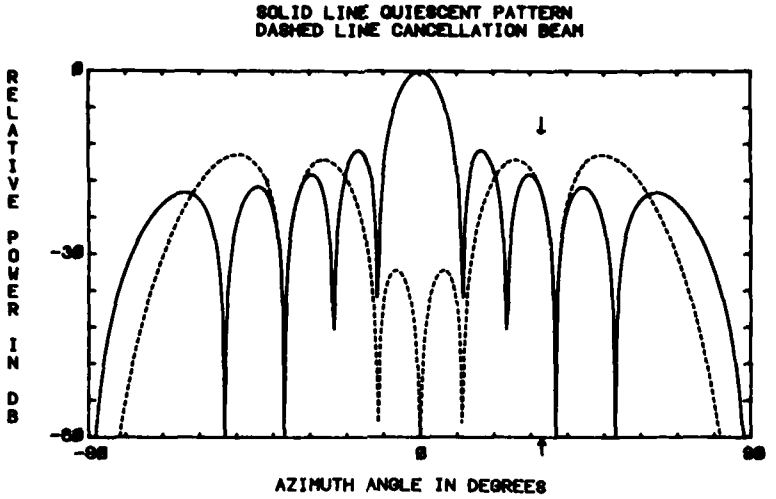

Figure 18c. Sum Channel Cancellation Beam From Simultaneous Sum and Difference Channel Phase-Only Nulling

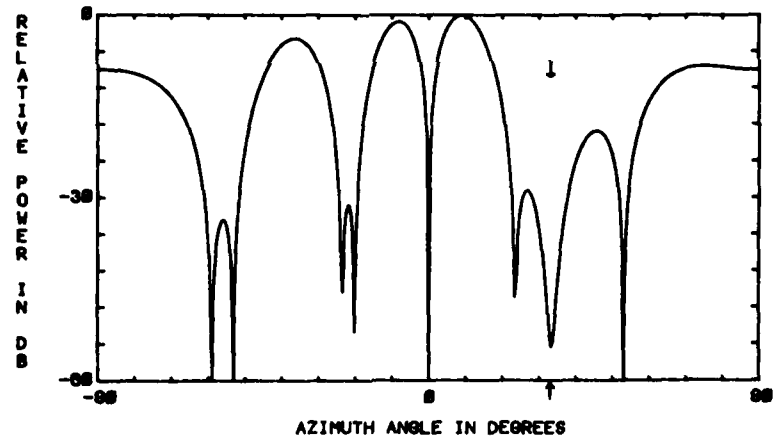

Figure 18d. Far Field Difference Pattern Due to Simultaneous Sum and Difference Channel Phase-Only Nulling

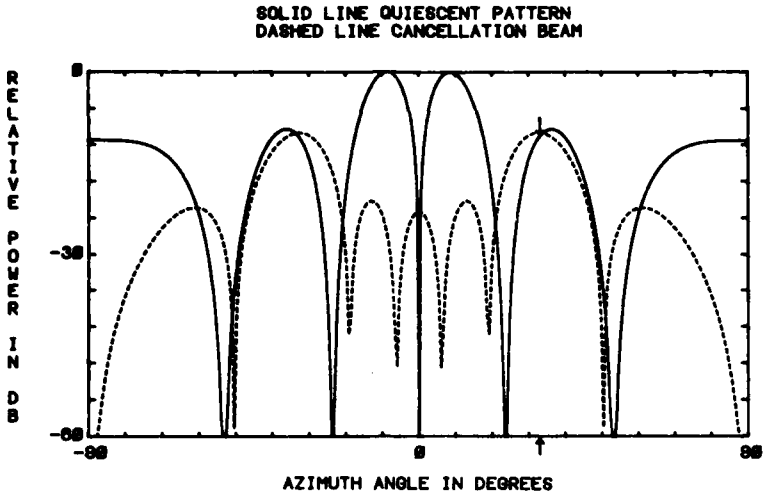

Figure 18e. Difference Channel Cancellation Beam From Simultaneous Sum and Difference Channel Phase-Only Nulling

The next set of computer runs tested low sidelobe distributions and multiple jammers. The sum channel had a 35 dB, $\bar{n} = 6$ Taylor distribution and the difference channel had a 35 dB, $\bar{n} = 6$ Bayliss distribution. One jammer was at 23° and the other at 50°. First, amplitude and phase nulling was tried in the sum channel, difference channel, and simultaneously. As in the previous cases, only the simultaneous nulling algorithm places nulls in the sum and difference patterns at the same time. These conditions were also used for phase-only nulling. Figures 19 to 25 demonstrate the multiple jammer scenario for a low sidelobe antenna.

A special case of interest is when the sum and difference patterns do not have the same sidelobe structure. Figures 26a and 26b show the results of simultaneous nulling in a uniform difference pattern and a 30 dB Chebychev sum pattern. In spite of the difference in sidelobe levels between the two patterns, each had a deep null at 33°. The resultant Chebychev pattern no longer has a -30 dB sidelobe level, but has sidelobes on the order of -18 dB. From this example, we can conclude that simultaneous nulling works for sum and difference patterns with completely different sidelobe structures. On the other hand, the adapted patterns have distorted mainbeams and sidelobe levels.

The simulation results shown in this section demonstrate that the nulling algorithms work. However, these results are only theoretical and have severe limitations for any practical implementations. The problems and limitations associated with simultaneous nulling are discussed in the next section.

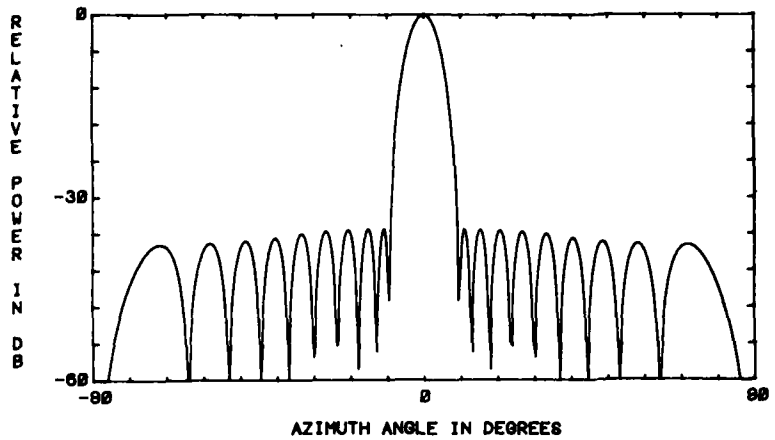

Figure 19a. Quiescent Far Field Sum Pattern of a 20-Element, 35 dB, $\bar{n}$ = 6 Taylor Array

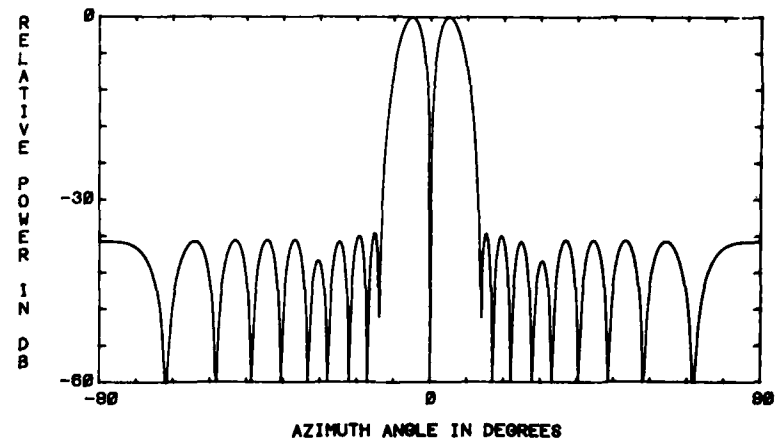

Figure 19b. Quiescent Difference Pattern of a 20-Element Array With a 35 dB, $\bar{n}$ = 6 Bayliss Distribution

	VARIABLE COMPLEX WEIGHTS		AMPLITUDE TAPERS	
ELEMENT	AMPLITUDE	PHASE	SUM CHAN	DIF CHANNEL
1	1.00000	0.00000	0.17026	−0.17909
2	1.00000	0.00000	0.22088	−0.31064
3	1.00000	0.00000	0.31299	−0.51854
4	1.00000	0.00000	0.43081	−0.73232
5	1.00000	0.00000	0.55793	−0.90304
6	1.00000	0.00000	0.68277	−1.00000
7	1.00000	0.00000	0.79770	−0.98841
8	1.00000	0.00000	0.89452	−0.83833
9	1.00000	0.00000	0.96409	−0.55771
10	1.00000	0.00000	1.00000	−0.19455
11	1.00000	0.00000	1.00000	0.19455
12	1.00000	0.00000	0.96409	0.55771
13	1.00000	0.00000	0.89452	0.83833
14	1.00000	0.00000	0.79770	0.98841
15	1.00000	0.00000	0.68277	1.00000
16	1.00000	0.00000	0.55793	0.90304
17	1.00000	0.00000	0.43081	0.73232
18	1.00000	0.00000	0.31299	0.51854
19	1.00000	0.00000	0.22088	0.31064
20	1.00000	0.00000	0.17026	0.17909

Figure 19c. Quiescent Taylor Sum and Bayliss Difference Distributions (35 dB sidelobes, $\bar{n} = 6$)

6. LIMITATIONS ON SIMULTANEOUS NULLING

The practical implementation of the simultaneous nulling algorithm has three basic problems. First, the jammer must be accurately located. This can be done by using either a separate antenna or by having the adaptive antenna take time out to search for jammers. The first idea requires an extra antenna and associated equipment. Considering the cost of the extra equipment, this option is undesirable. The second idea significantly cuts down the amount of time the radar has for tracking and detecting targets. Under many situations, this alternative is not acceptable. In any case, in a multiple jammer environment, the antenna may not be able to accurately locate each jamming source. Thus, adaptive algorithms that need the jammer location in order to place the null are probably not practical to implement.

A second problem with the algorithm is caused by hardware tolerances and the environment. Equipment such as phase shifters, power dividers, transmission lines, and antenna elements create phase and amplitude errors. Also, environmental effects like mutual coupling, multipath, and scattering add unwanted errors to the received signals. These errors appear in the far field antenna pattern as higher sidelobes and filled-in nulls.

	VARIABLE COMPLEX WEIGHTS		VARIABLE WEIGHTS TIMES AMPLITUDE TAPERS	
ELEMENT	AMPLITUDE	PHASE	SUM CHAN	DIF CHANNEL
1	0.99812	–0.00228	0.16994	–0.17875
2	1.00152	0.00161	0.22122	–0.31111
3	0.99654	–0.00481	0.31191	–0.51675
4	0.99799	0.01049	0.42994	–0.73085
5	1.00976	–0.00565	0.56337	–0.91186
6	0.99300	0.00166	0.67799	–0.99300
7	1.01147	–0.00535	0.80685	–0.99974
8	0.97940	–0.00639	0.87610	–0.82106
9	1.00872	0.01982	0.97249	–0.56257
10	1.00229	–0.01262	1.00229	–0.19500
11	1.00229	0.01262	1.00229	0.19500
12	1.00872	–0.01982	0.97249	0.56257
13	0.97940	0.00639	0.87610	0.82106
14	1.01147	0.00535	0.80685	0.99974
15	0.99300	–0.00166	0.67799	0.99300
16	1.00976	0.00565	0.56337	0.91186
17	0.99799	–0.01049	0.42994	0.73085
18	0.99654	0.00481	0.31191	0.51675
19	1.00152	–0.00161	0.22122	0.31111
20	0.99812	0.00228	0.16994	0.17875

Figure 20a. Adapted Weights From Amplitude and Phase Nulling in the Sum Channel

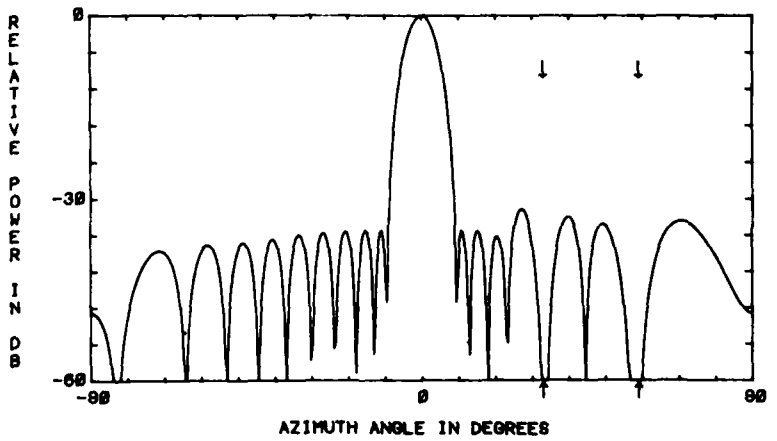

Figure 20b. Far Field Sum Pattern Due to Amplitude and Phase Nulling in the Sum Channel

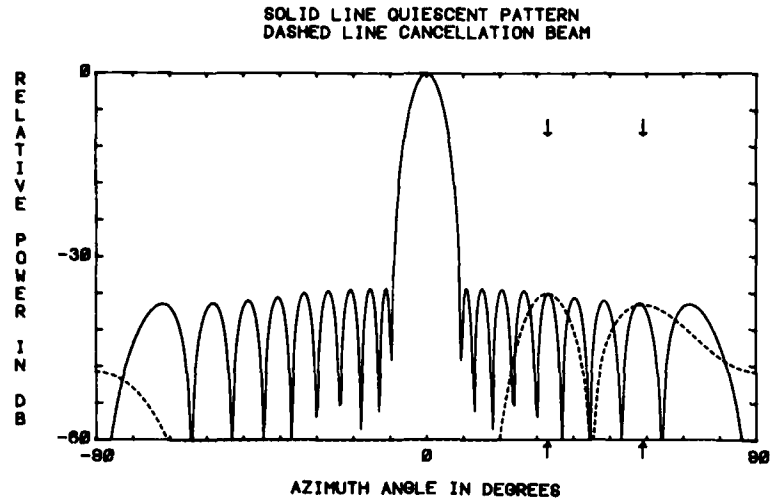

Figure 20c. Cancellation Beam From Amplitude and Phase Nulling in the Sum Channel

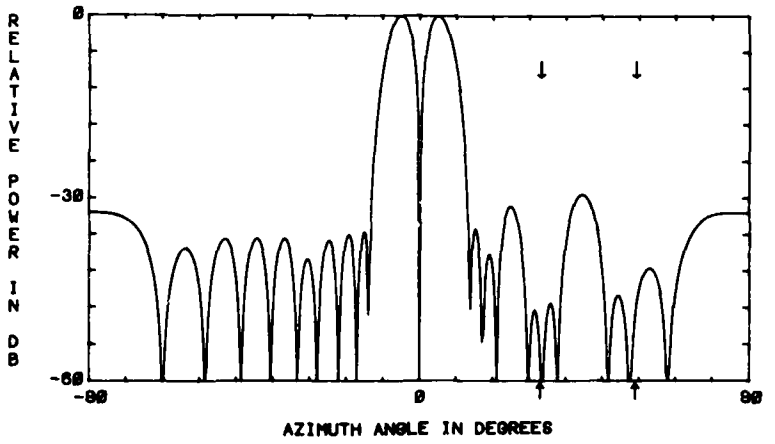

Figure 20d. Far Field Difference Pattern Due to Amplitude and Phase Nulling in the Sum Channel

ELEMENT	VARIABLE COMPLEX WEIGHTS AMPLITUDE	PHASE	VARIABLE WEIGHTS TIMES AMPLITUDE TAPERS SUM CHAN	DIF CHANNEL
1	0.99858	−0.00037	0.17002	−0.17883
2	0.99864	0.00072	0.22058	−0.31022
3	0.99926	0.00455	0.31276	−0.51816
4	1.00835	0.00128	0.43441	−0.73843
5	1.00104	−0.00849	0.55851	−0.90399
6	0.99578	−0.00299	0.67989	−0.89578
7	0.99256	0.00000	0.79177	−0.98106
8	0.99934	0.00939	0.89393	−0.83777
9	1.00587	0.00007	0.96975	−0.56098
10	1.00029	−0.00116	1.00029	−0.19461
11	1.00029	0.00116	1.00029	0.19461
12	1.00587	−0.00007	0.96975	0.56098
13	0.99934	−0.00939	0.89393	0.83777
14	0.99256	0.00000	0.79177	0.98106
15	0.99578	0.00299	0.67989	0.99578
16	1.00104	0.00849	0.55851	0.90399
17	1.00835	−0.00128	0.43441	0.73843
18	0.99926	−0.00455	0.31276	0.51816
19	0.99864	−0.00072	0.22058	0.31022
20	0.99858	0.00037	0.17002	0.17883

Figure 21a. Adapted Weights From Amplitude and Phase Nulling in the Difference Channel

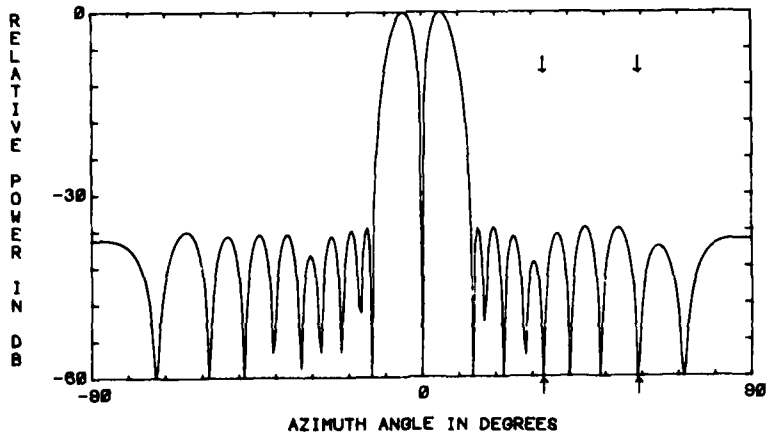

Figure 21b. Far Field Difference Pattern Due to Amplitude and Phase Nulling in the Difference Channel

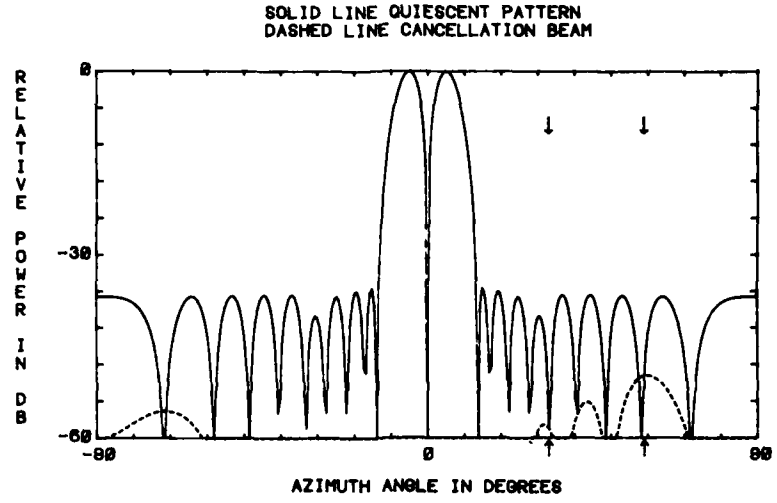

Figure 21c. Cancellation Beam From Amplitude and Phase Nulling in the Difference Channel

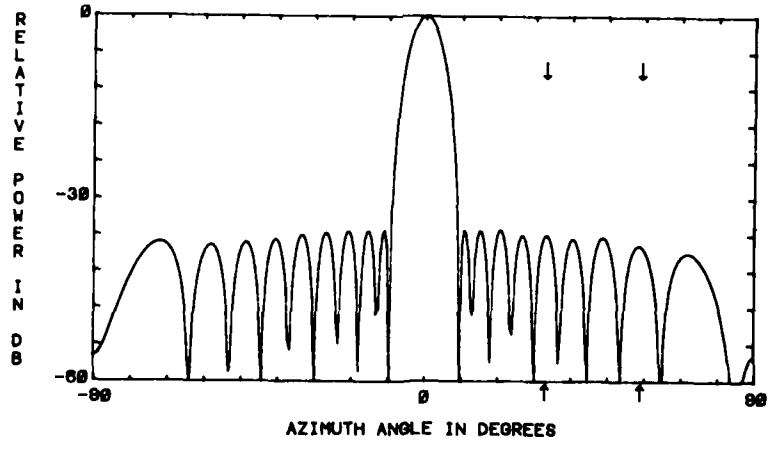

Figure 21d. Far Field Sum Pattern Due to Amplitude and Phase Nulling in the Difference Channel

	VARIABLE COMPLEX WEIGHTS		VARIABLE WEIGHTS TIMES AMPLITUDE TAPERS	
ELEMENT	AMPLITUDE	PHASE	SUM CHAN	DIF CHANNEL
1	0.99671	−0.00266	0.16970	−0.17850
2	1.00016	0.00233	0.22092	−0.31069
3	0.99577	−0.00025	0.31167	−0.51635
4	1.00635	0.01168	0.43354	−0.73697
5	1.01085	−0.01405	0.56398	−0.91284
6	0.98878	−0.00134	0.67511	−0.98878
7	1.00404	−0.00539	0.80092	−0.99239
8	0.97868	0.00319	0.87545	−0.82046
9	1.01459	0.01977	0.97815	−0.56585
10	1.00260	−0.01378	1.00260	−0.19505
11	1.00260	0.01378	1.00260	0.19505
12	1.01459	−0.01977	0.97815	0.56585
13	0.97868	−0.00319	0.87545	0.82046
14	1.00404	0.00539	0.80092	0.99239
15	0.98878	0.00134	0.67511	0.98878
16	1.01085	0.01405	0.56398	0.91284
17	1.00635	−0.01168	0.43354	0.73697
18	0.99577	0.00025	0.31167	0.51635
19	1.00016	−0.00233	0.22091	0.31069
20	0.99671	0.00266	0.16970	0.17850

Figure 22a. Adapted Weights From Simultaneous Amplitude and Phase Nulling in the Sum and Difference Channels

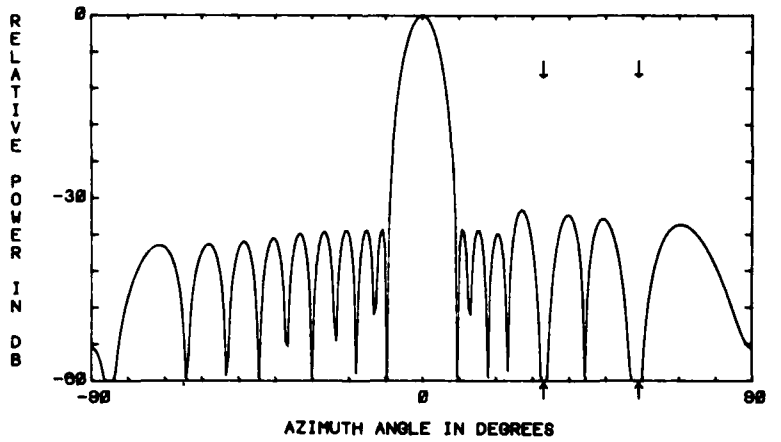

Figure 22b. Far Field Sum Pattern Due to Simultaneous Amplitude and Phase Nulling in the Sum and Difference Channels

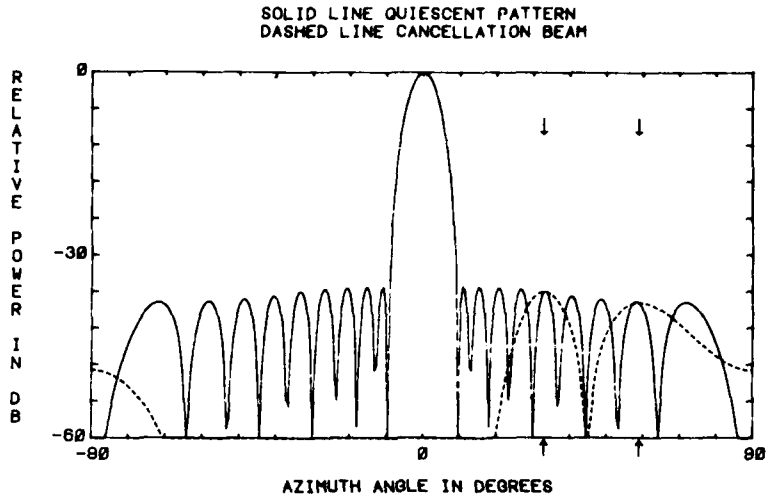

Figure 22c. Sum Channel Cancellation Beam From Amplitude and Phase Nulling in the Sum and Difference Channels Simultaneously

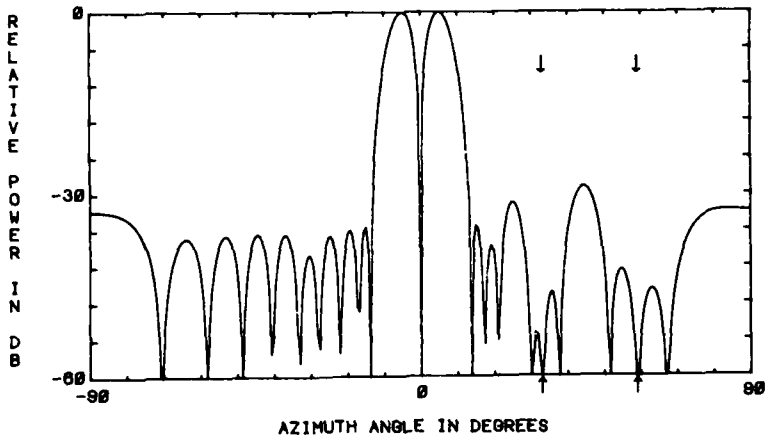

Figure 22d. Far Field Difference Pattern Due to Amplitude and Phase Nulling in the Sum and Difference Channels Simultaneously

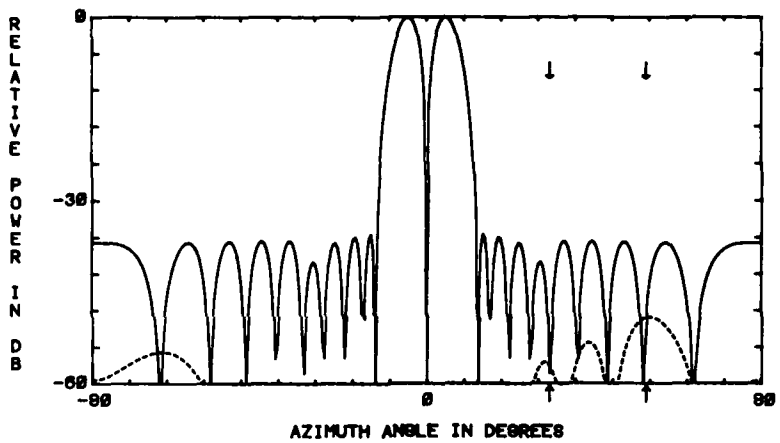

Figure 22e. Difference Channel Cancellation Beam From Amplitude and Phase Nulling in the Sum and Difference Channels Simultaneously

ELEMENT	PHASE SHIFT
1	–0.00454
2	0.00324
3	–0.00959
4	0.02086
5	–0.01142
6	0.00334
7	–0.01074
8	–0.01251
9	0.03983
10	–0.02533
11	0.02533
12	–0.03983
13	0.01251
14	0.01074
15	–0.00334
16	0.01142
17	–0.01086
18	-0.00959
19	–0.00324
20	0.00454

Figure 23a. Adapted Weights From Phase-Only Nulling in the Sum Channel

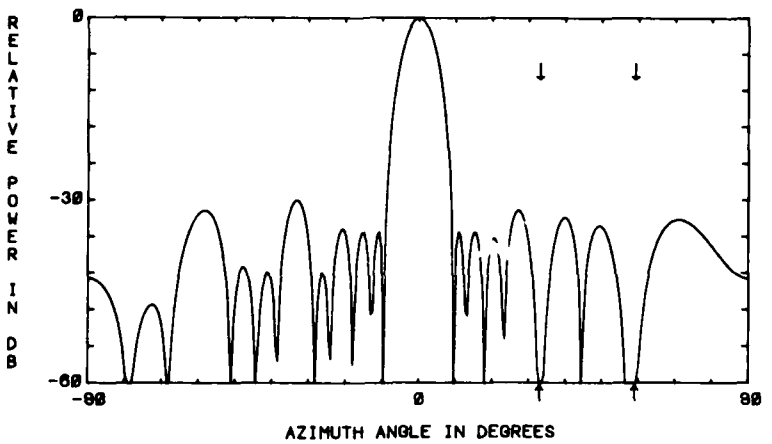

Figure 23b. Far Field Sum Pattern Due to Phase-Only Nulling in the Sum Channel

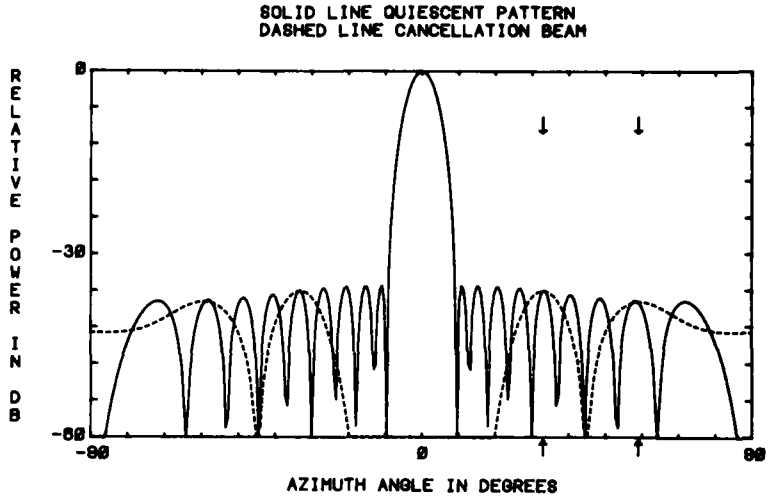

Figure 23c. Sum Channel Cancellation Beam From Phase-Only Nulling in the Sum Channel

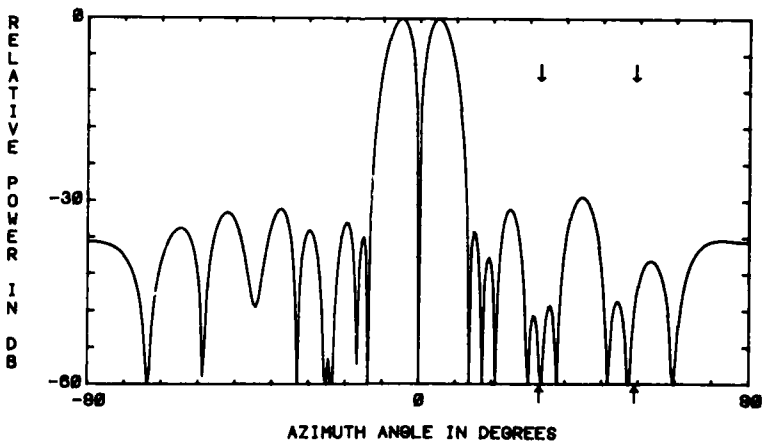

Figure 23d. Far Field Difference Pattern Due to Phase-Only Nulling in the Sum Channel

ELEMENT	PHASE SHIFT
1	–0.00094
2	0.00166
3	0.00898
4	0.00240
5	–0.01639
6	–0.00700
7	0.00115
8	0.01794
9	0.00055
10	–0.00238
11	0.00238
12	–0.00055
13	–0.01794
14	–0.00115
15	0.00700
16	0.01639
17	–0.00240
18	–0.00898
19	–0.00166
20	0.00094

Figure 24a. Adapted Weights From Phase-Only Nulling in the Difference Channel

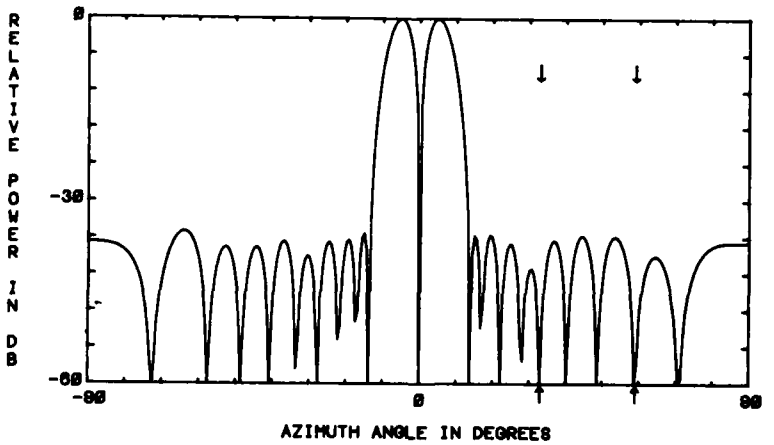

Figure 24b. Far Field Difference Pattern Due to Phase-Only Nulling in the Difference Channel

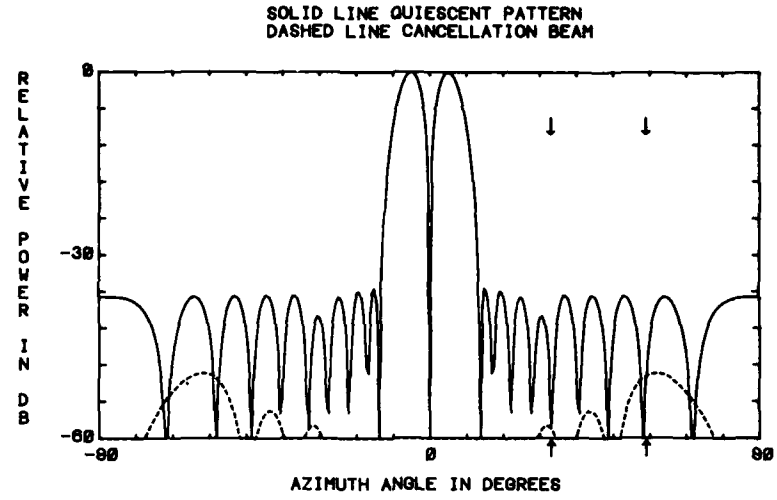

Figure 24c. Difference Channel Cancellation Beam From Phase-Only Nulling in the Difference Channel

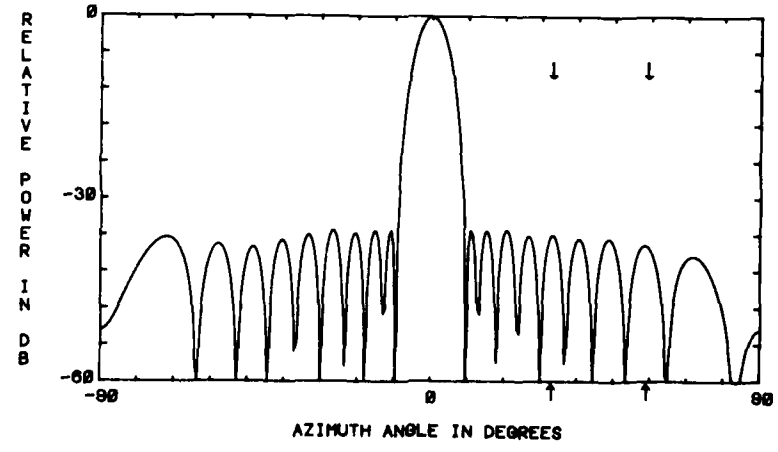

Figure 24d. Far Field Sum Pattern Due to Phase-Only Nulling in the Difference Channel

ELEMENT	PHASE SHIFT
1	–0.00530
2	0.00473
3	–0.00058
4	0.02356
5	–0.02857
6	–0.00248
7	–0.01074
8	0.00618
9	0.04015
10	–0.02796
11	0.02796
12	–0.04015
13	–0.00618
14	0.01074
15	0.00248
16	0.02857
17	–0.02356
18	0.00058
19	–0.00473
20	0.00530

Figure 25a. Adapted Weights From Phase-Only Nulling in the Sum and Difference Channels Simultaneously

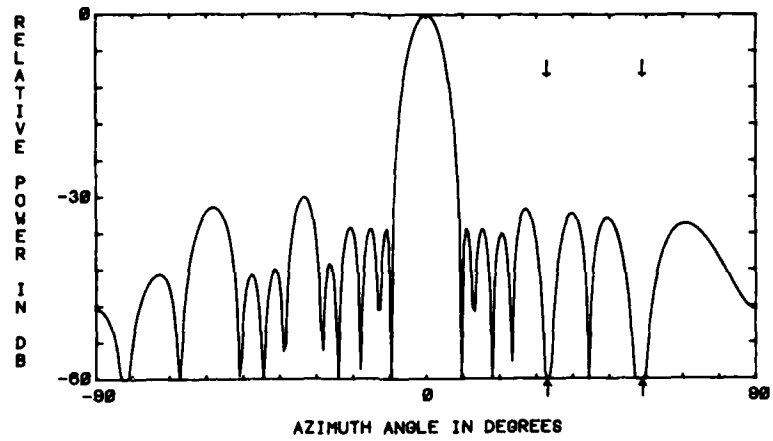

Figure 25b. Far Field Sum Pattern Due to Phase-Only Nulling in the Sum and Difference Channels Simultaneously

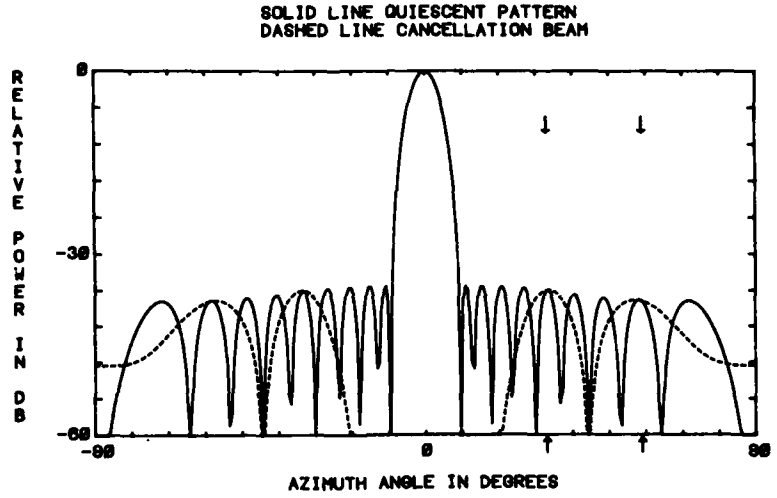

Figure 25c. Sum Channel Cancellation Beam From Phase-Only Nulling in the Sum and Difference Channels Simultaneously

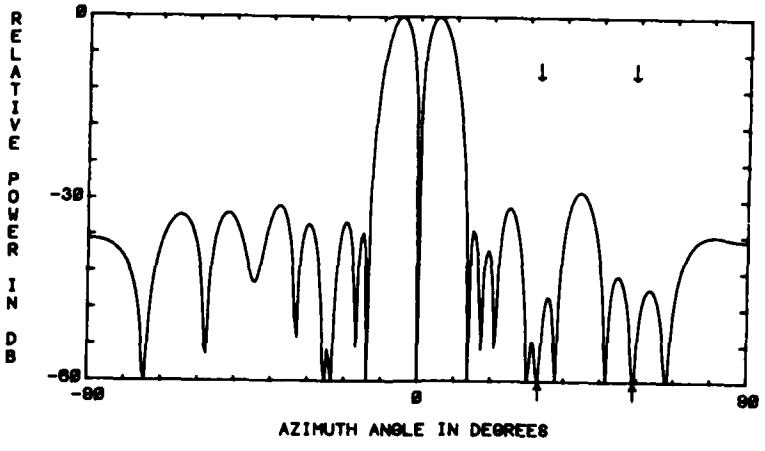

Figure 25d. Far Field Difference Pattern Due to Phase-Only Nulling in the Sum and Difference Channels Simultaneously

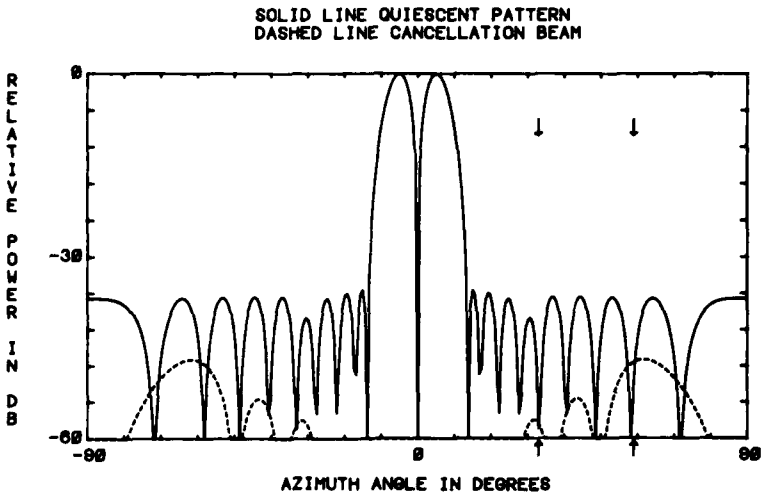

Figure 25e. Difference Channel Cancellation Beam From Phase-Only Nulling in the Sum and Difference Channels Simultaneously

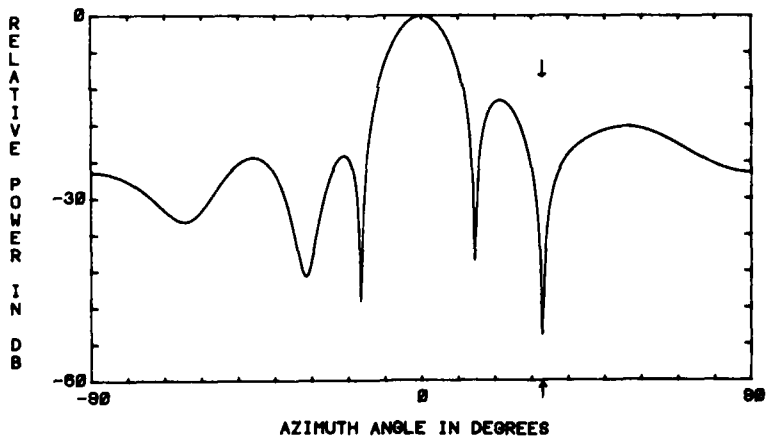

Figure 26a. Sum Pattern Resulting From Simultaneous Nulling in a 30 dB Chebychev Sum Pattern and a Uniform Difference Pattern

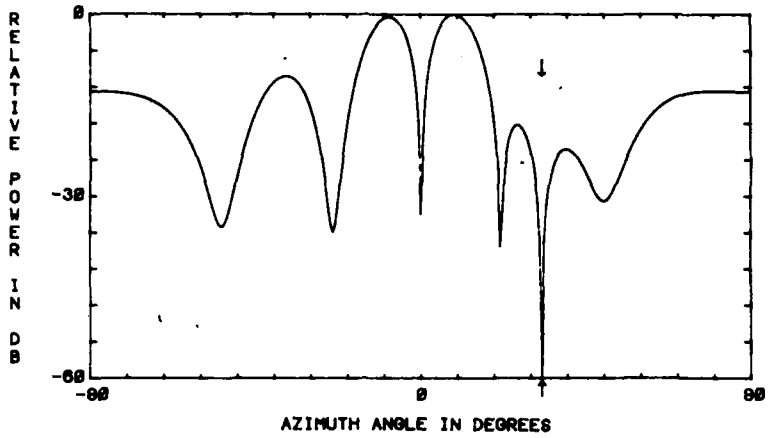

Figure 26b. Difference Pattern Resulting From Simultaneous Nulling in a 30 dB Chebychev Sum Pattern and a Uniform Difference Pattern

Two types of phased array errors of particular importance are correlated and uncorrelated random errors. Uncorrelated errors vary randomly from element to element. These are generally caused by component tolerances. Correlated errors result from groups of elements in which each element has a related error, but the errors are independent from group to group. These errors slowly vary across the aperture and are due to uneven heating, bending, edge effects, subarrays, and so on.

An antenna pattern consists of an error free pattern plus a pattern due to errors. The error pattern has a very wide mainbeam, like an element pattern (cosine shaped) Generally, the errors are small and do not affect the "high" sidelobes or mainbeam. Thus, close to the mainbeam the deterministic sidelobe pattern dominates and far from the mainbeam the error pattern dominates (assuming the sidelobes decay going away from the mainbeam). The lower the sidelobes, the more the errors dominate.

The simultaneous nulling algorithm generates a cancellation beam for a perfect antenna. This cancellation beam will not usually work for a non-ideal array. The non-ideal array has higher average sidelobe levels than an ideal array. Equation (135) statistically calculates the average sidelobe level for uncorrelated random errors.[9]

$$S = \frac{(1 - Pe) + \overline{\Delta}^2 + \overline{\delta}^2 Pe}{N \eta_T Pe(1 - \overline{\delta}^2)} \qquad (135)$$

9. Brookner, E. (n.d.) Antenna array fundamentals. Taken from course notes from Microwave Journal Intensive Course, Practical Phased-Array Systems.

where

S = average far-out sidelobe power level,

N = number of elements,

P_e = probability of survival of i^{th} rading element (calculated from MTBF of an element),

η_T = taper efficiency for a linear array, that is,

$$\eta_T = \frac{(\sum_{i=1}^{N} I_i)^2}{N \sum_{i=1}^{N} I_i^2}$$

where

I_i = amplitude weight at element i,

$\overline{\Delta}^2$ = mean square value of element amplitude error,

$\overline{\Delta}^2 = \overline{\Delta}^2_{AMP} + \overline{\Delta}^2_{RAD} + \overline{\Delta}^2_{Q}$

Δ^2_{AMP} = mean square amplifier and phase shifter fractional amplitude errors,

$\overline{\Delta}^2_{RAD}$ = mean square fractional deviation of radiation element voltage pattern from nominal value,

$\overline{\Delta}^2_{Q}$ = quantization of amplitude weights,

$\overline{\delta}^2$ = mean square value of element phase error,

$$\overline{\delta}^2 = \overline{\delta}^2_{MECH} + \overline{\delta}^2_{PH} + \overline{\delta}^2_{POL} + \overline{\delta}^2_{Q},$$

σ = standard deviation of error. A gaussian distribution with a mean of zero is assumed.

$\overline{\delta}^2_{MECH}$ = mechanical deviation error, or,

$$\overline{\delta}^2_{MECH} = (2\pi/\lambda)^2 \sigma_{MECH}$$

where

λ = wavelength,

$$\sigma^2_{MECH} = (\Delta \overline{x}_n)^2 = (\Delta \overline{y}_n)^2,$$

$\Delta \bar{x}_n$ = deviation of element n in x-direction ,

$\Delta \bar{y}_n$ = deviation of element n in y-direction,

$\bar{\delta}^2_{PH} = \sigma^2_{PH}$ = deviation in the plane of the aperture in the same units as λ ,

$\bar{\delta}^2_{POL} \leqq \sigma^2$ = variance of α, the rotation angle error of the dipole. This error is usually ignored because it is very small.

$\bar{\delta}^2_Q = \frac{\pi^2}{3 \times 2^{2P}}$ P = number of bits in phase shifter.

In general, the lower the sidelobes, the greater the array amplitude taper, and the smaller η_T. Also, the more elements, the less effects the errors have on sidelobe level.

As an example, consider a 100-element array with the following tolerances:

$$\sigma_A = 0.043$$

$$\eta_T = 85 \text{ percent}$$

$$\sigma_P = 3.58°$$

$$P_e \approx 1$$

$$S = \frac{\bar{\Delta}^2 + \bar{\delta}^2}{(1 - \bar{\delta}^2)\eta_T N} = \frac{0.00185 + 0.0039}{(1 - 0.0039)(0.85)(100)} = 0.0000679$$

$$= 41.68 \text{ dB below peak of mainbeam.}$$

Some other examples of the effects of uncorrelated random errors are found in Appendix B. The effects of uncorrelated random errors on the simultaneous nulling process are demonstrated in Figures 27 through 30. Since the adaptive weight changes are very small and must have a high degree of accuracy, errors significantly impact the array's nulling capability. Usually, the greatest errors are found in the phase shifters. Notice how the null fills in as the number of bits decrease in Figures 27 and 28. All the phase shifts are smaller than the least significant bit on a 4-bit phase shifter. The next figure shows the pattern after an element failure. One element failure in a small low sidelobe array has devastating results. Figures 30a-30c are cases of random errors applied to the array. These figures demonstrate the tight tolerances required to accurately create a null in antenna patterns.

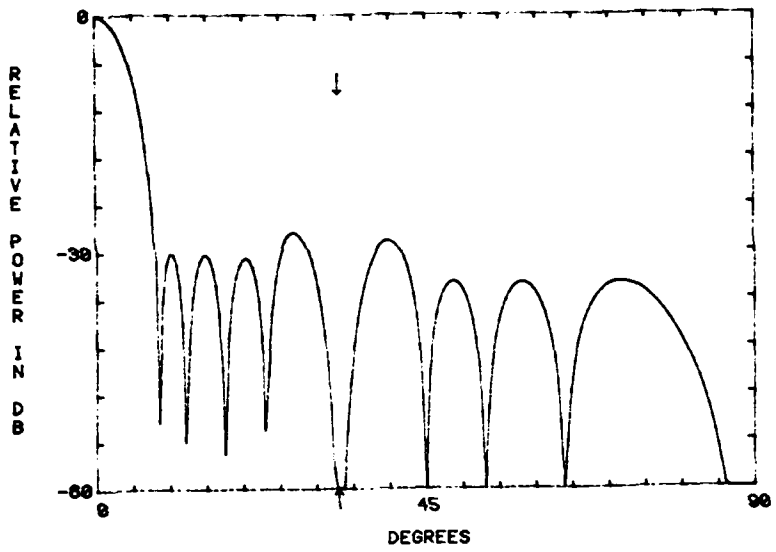

Figure 27a. Phase-Only Nulling in the Sum and Difference Channels Simultaneously on a 30 dB, $\bar{n} = 6$ Taylor Pattern With No Errors

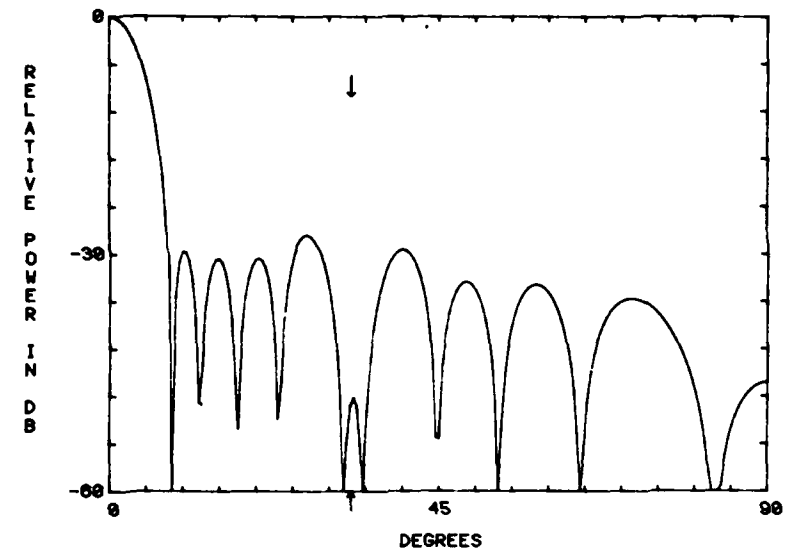

Figure 27b. Phase-Only Nulling in the Sum and Difference Channels Simultaneously on a 30 dB, $\bar{n} = 6$ Taylor Pattern With 9-Bit Phase Shifters

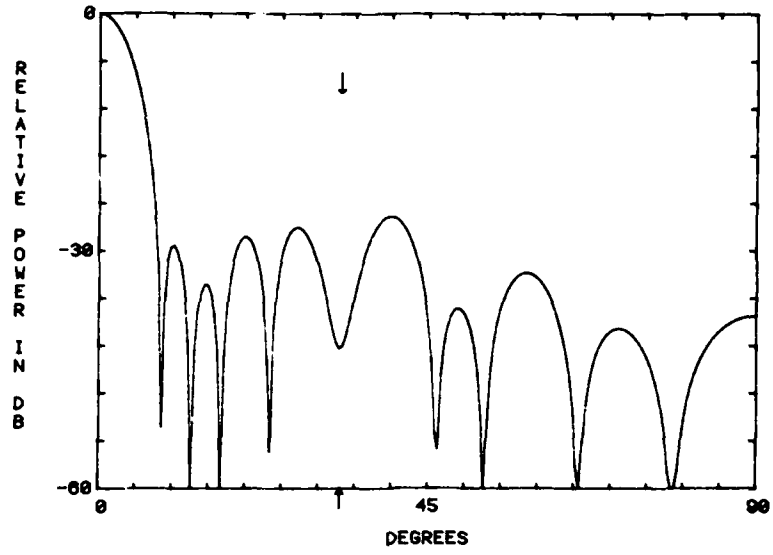

Figure 27c. Phase-Only Nulling in the Sum and Difference Channels Simultaneously on a 30 dB, $\bar{n}$ = 6 Taylor Pattern With 6-Bit Phase Shifters

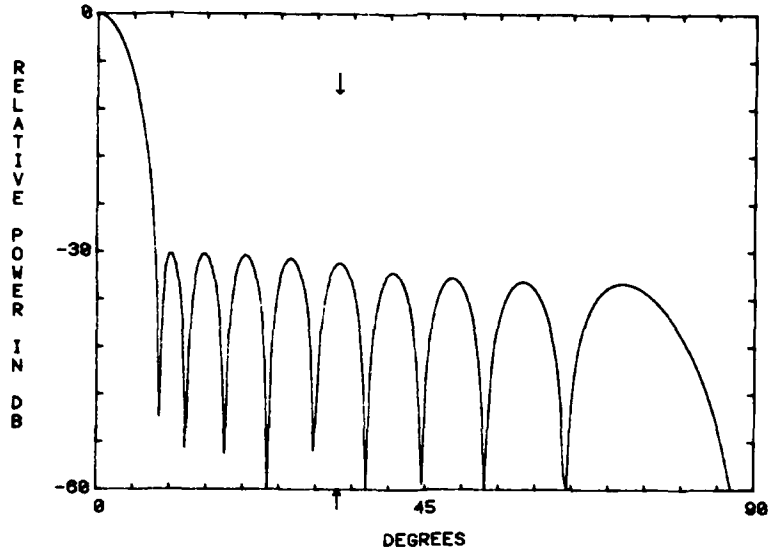

Figure 27d. Phase-Only Nulling in the Sum and Difference Channels Simultaneously on a 30 dB, $\bar{n}$ = 6 Taylor Pattern With 4-Bit Phase Shifters

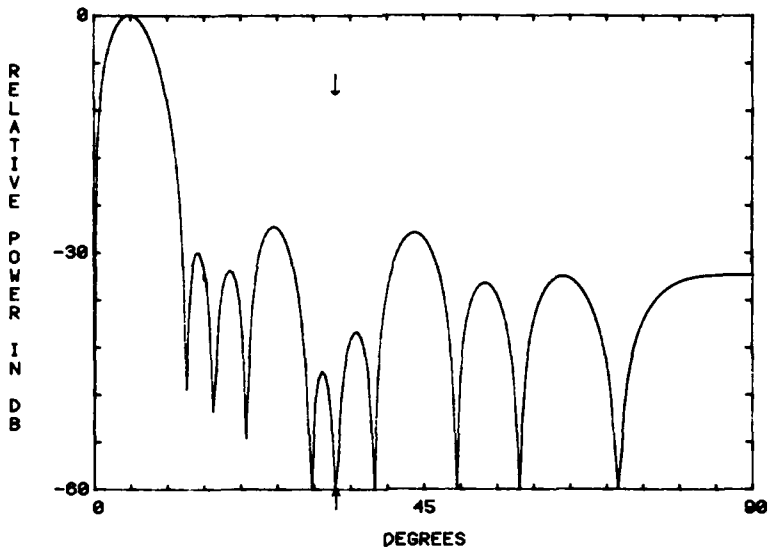

Figure 28a. Phase-Only Nulling in the Sum and Difference Channels Simultaneously on a 30 dB, $\bar{n}$ = 6 Bayliss Pattern With No Errors

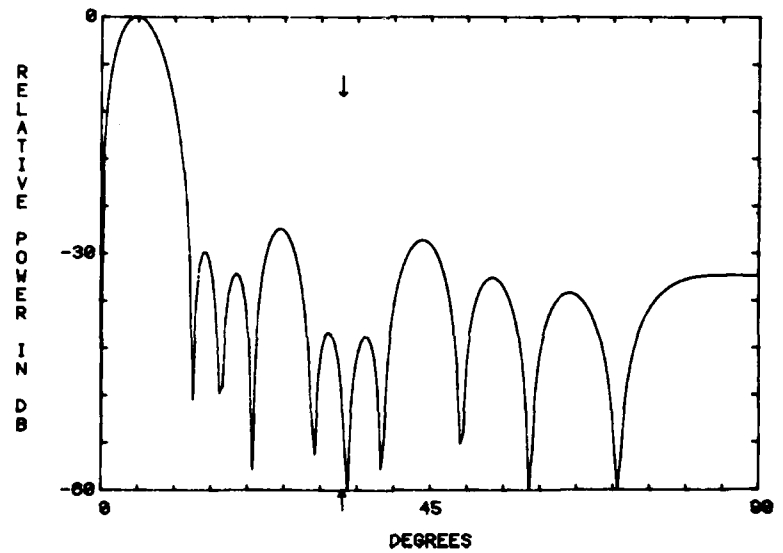

Figure 28b. Phase-Only Nulling in the Sum and Difference Channels Simultaneously on a 30 dB, $\bar{n}$ = 6 Bayliss Pattern With 8-Bit Phase Shifters

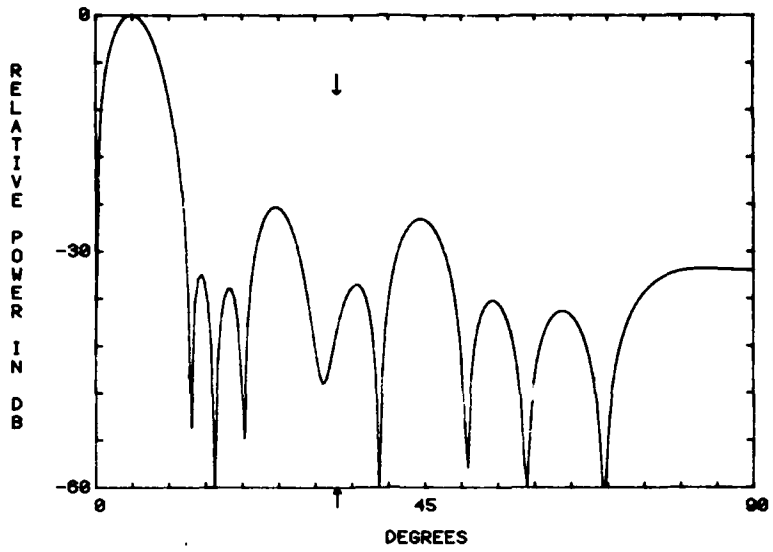

Figure 28c. Phase-Only Nulling in the Sum and Difference Channels Simultaneously on a 30 dB, $\bar{n}$ = 6 Bayliss Pattern With 6-Bit Phase Shifters

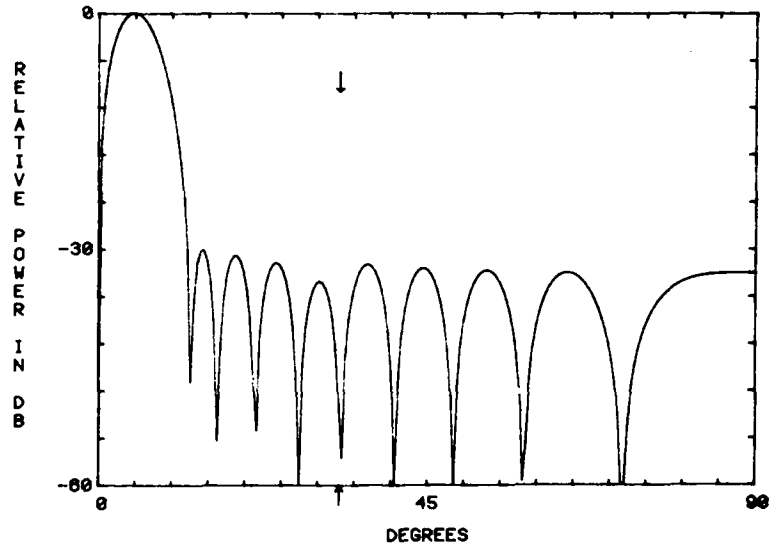

Figure 28d. Phase-Only Nulling in the Sum and Difference Channels Simultaneously on a 30 dB, $\bar{n}$ = 6 Bayliss Pattern With 4-Bit Phase Shifters

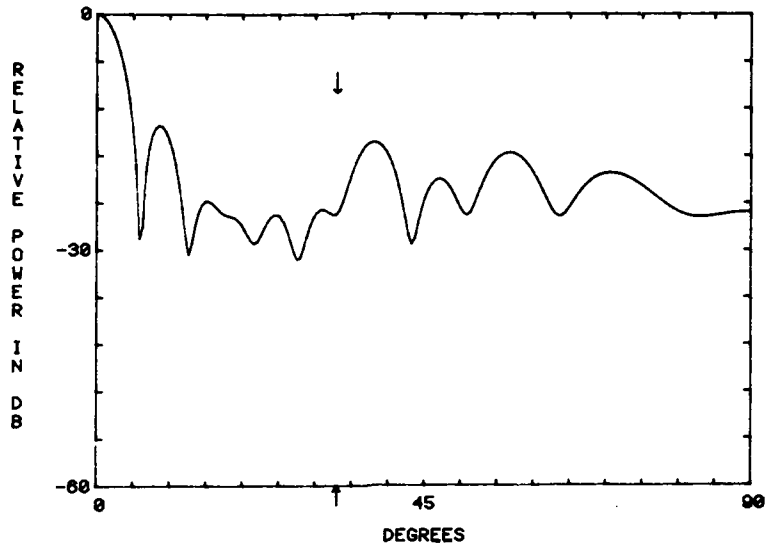

Figure 29. Phase-Only Nulling in the Sum and Difference Channels Simultaneously on a 30 dB, $\bar{n} = 6$ Taylor Pattern With Number 2 Element Failure

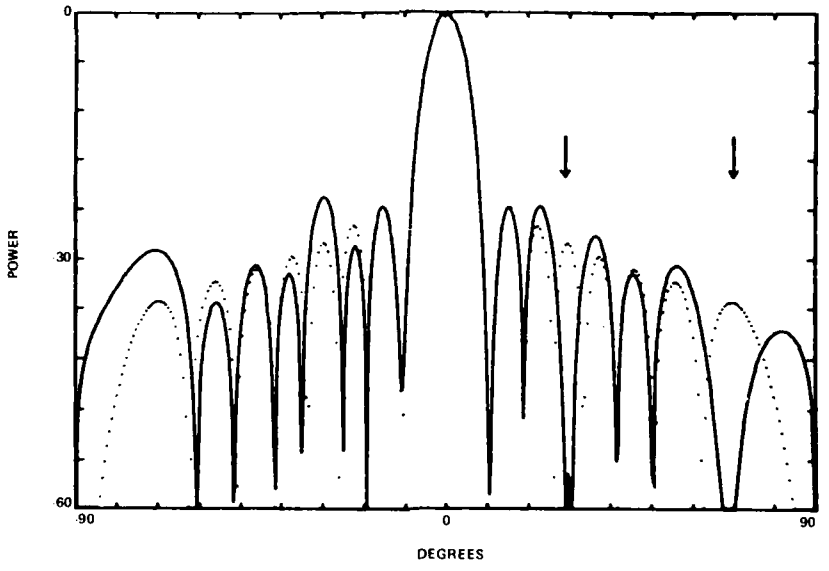

Figure 30a. Phase-Only Nulling in an 18-Element Low Sidelobe Array With No Errors

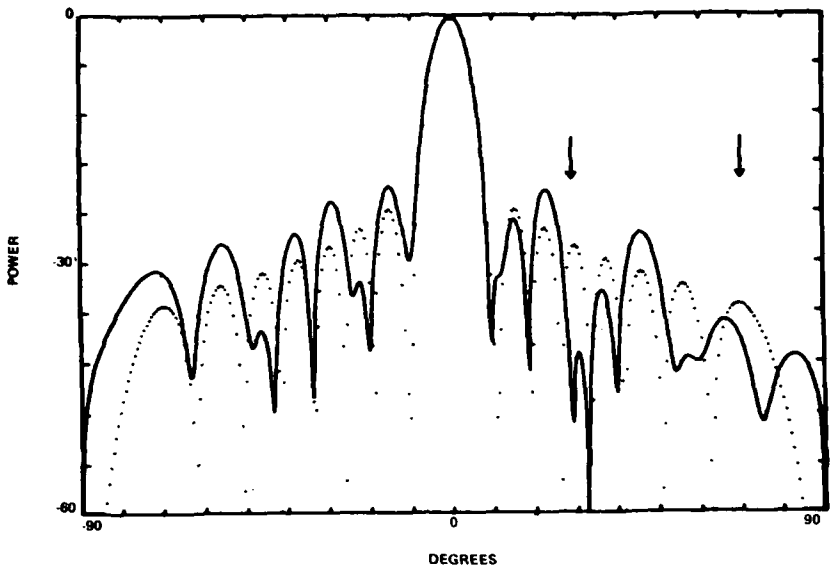

Figure 30b. Phase-Only Nulling in an 18-Element Low Sidelobe Array With 0.1 Percent Amplitude Error, 1° Phase Error, 0.0001λ Position Error, and 8-Bit Phase Shifters

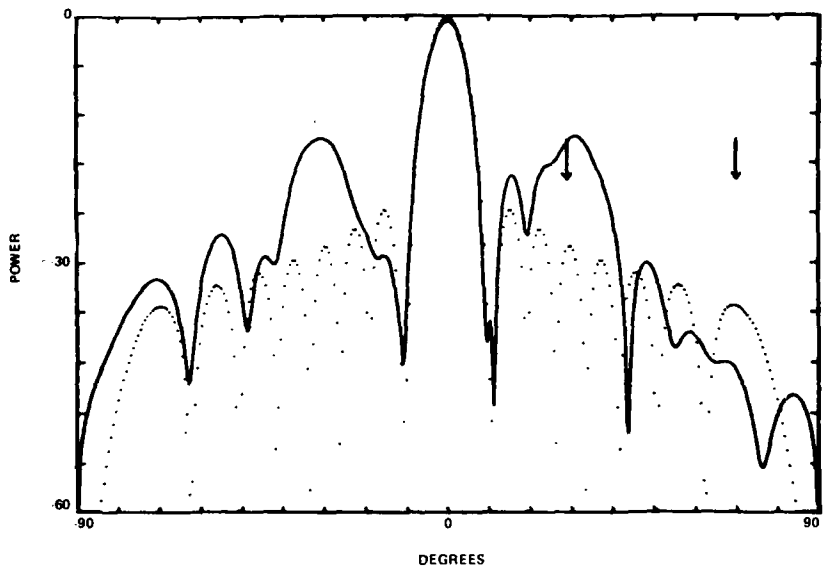

Figure 30c. Phase-Only Nulling in an 18-Element Low Sidelobe Array With 2 Percent Amplitude Error, 4° Phase Error, 0.0001λ position Error, and 8-Bit Phase Shifters

The analysis of correlated errors is similar to that of uncorrelated errors. For the uncorrelated errors the entire antenna can be thought of as N correlation regions. In the analysis of correlated errors, the antenna is divided into several regions. The errors within a region are correlated while the errors from region to region are uncorrelated. Again we can think of the actual antenna pattern as being made up of several patterns: the error-free pattern, the pattern due to uncorrelated errors, and the pattern due to correlated errors. Unlike the uncorrelated errors, the effects of the correlated errors are restricted to the vicinity of the mainbeam. Thus, correlated errors are predominant close to the mainbeam, and uncorrelated errors are predominant in the far-out sidelobe regions. Equation (136) determines the effect of correlated errors on the average sidelobe level of an array.[9]

$$S = \frac{(1 - Pe) + \overline{\Delta}^2 + \overline{\delta}^2 Pe}{\eta_T n_s \; Pe(1 - \overline{\delta}^2)} \left(\frac{1}{\eta_T n_s} \right) \tag{136}$$

where

n_s = number of correlation regions,

δ and Δ are identical for all radiating elements within a correlation region,

N_s = number of elements within correlation region, and

$N = n_s N_s$.

No computer runs were made to demonstrate the effects of correlated random errors on simultaneous nulling.

The final major problem with the simultaneous nulling arises from the inherent limitations of the phase-only nulling approach. As mentioned earlier, phase-only nulling produces two equal amplitude, out-of-phase cancellation beams, one on each side of the mainbeam. These cancellation beams present significant problems with jammers that are symmetrical about the mainbeam and jammers in the mainbeam.

Figures 31a-31d demonstrate the problem with symmetrical jammers. The phase-only nulling algorithm does not work for perfectly symmetrical jammers. One cancellation beam subtracts from the left side of the mainbeam and adds to the right side, while the other dual cancellation beam tries to add to the left side and subtract from the right. As the jammers become less symmetrical, the nulling performance improves. As a rule of thumb, phase-only nulling works when nulls are not placed in two symmetrical sidelobes.

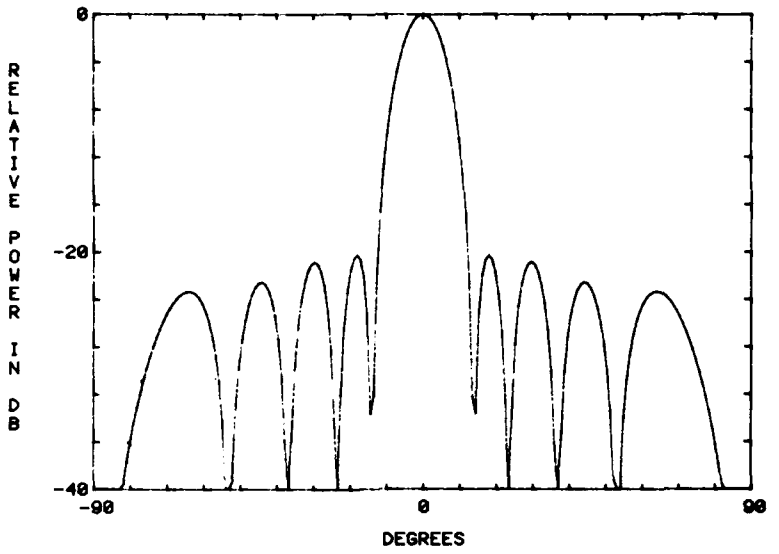

Figure 31a. Quiescent 10-Element, 20 dB, $\bar{n}$ = 3 Taylor Sum Pattern

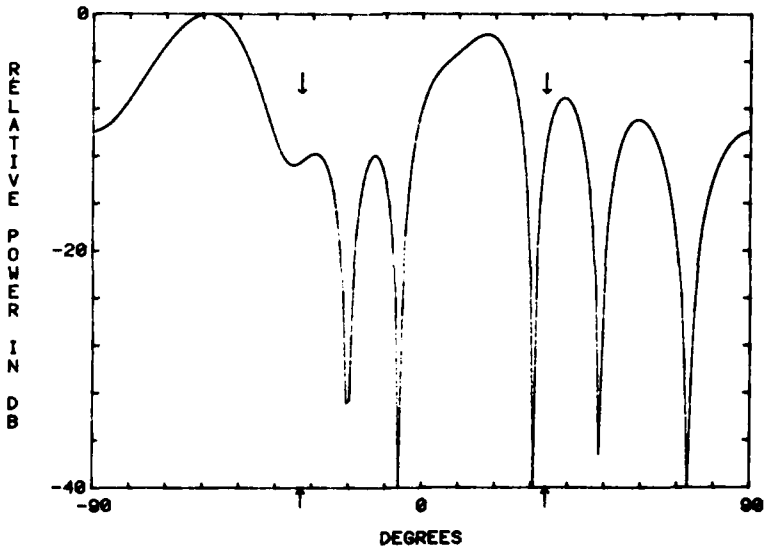

Figure 31b. Phase-Only Nulling With Nearly Symmetrical Jammers at -33 and -34°

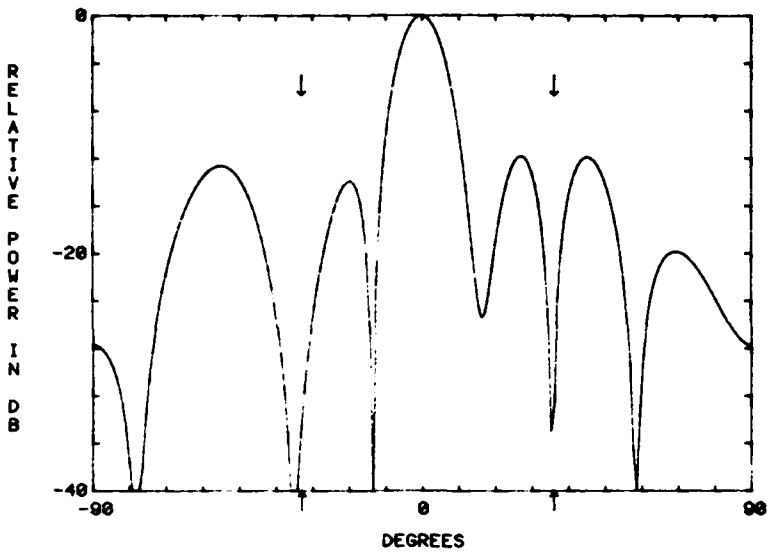

Figure 31c. Phase-Only Nulling With Nearly Symmetrical Jammers at -33 and -36°

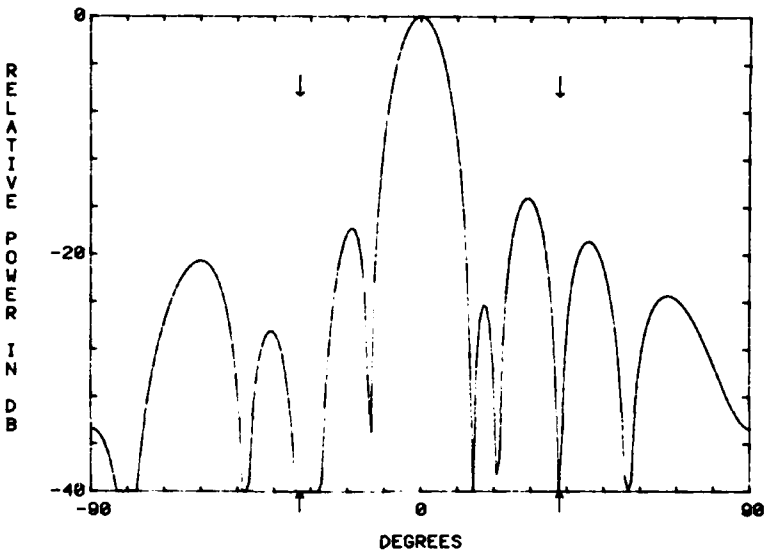

Figure 31d. Phase-Only Nulling With Nearly Symmetrical Jammers at -33 and -38°

Phase-only nulling gives poor results in the mainbeam. One lobe of the cancellation beam adds to one side of the mainbeam and the other cancellation lobe subtracts from the other side of the mainbeam. Figures 32a-32d depict the results.

The nulling results from this section appear in Table 3.

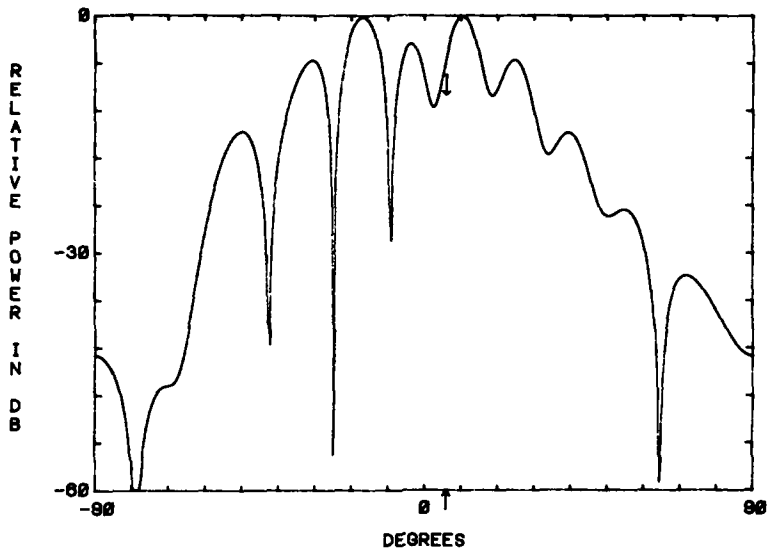

Figure 32a. Phase-Only Nulling in the Sum and Difference Channels Simultaneously in the Mainbeam of a Sum Pattern at 5°

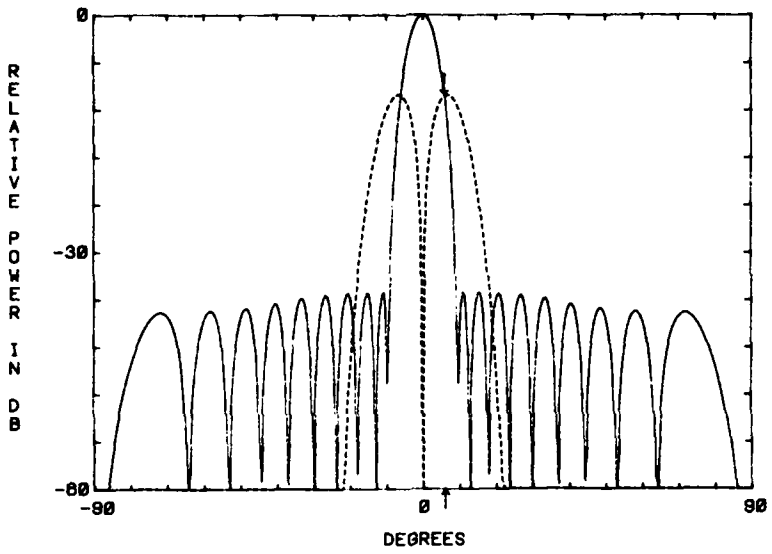

Figure 32b. Cancellation Beam From Phase-Only Nulling in the Sum and Difference Channels Simultaneously in the Mainbeam of a Sum Pattern

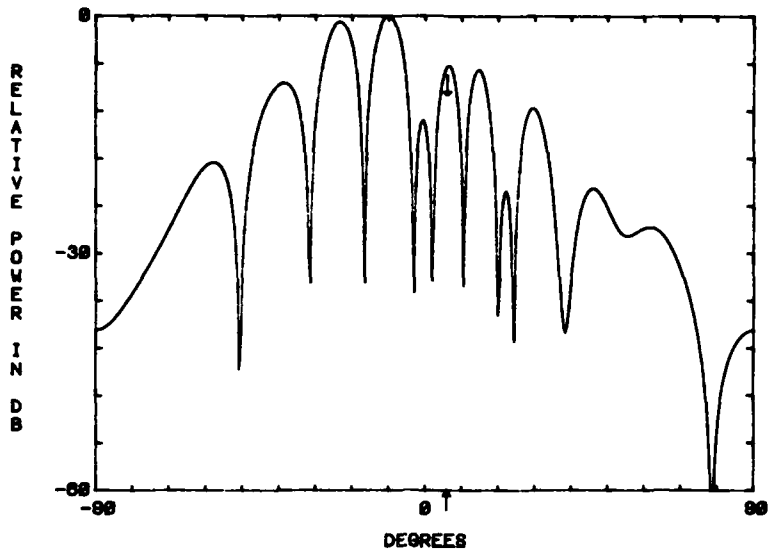

Figure 32c. Phase-Only Nulling in the Sum and Difference Channels Simultaneously With a Jammer in the Mainbeam of the Difference Pattern at 5°

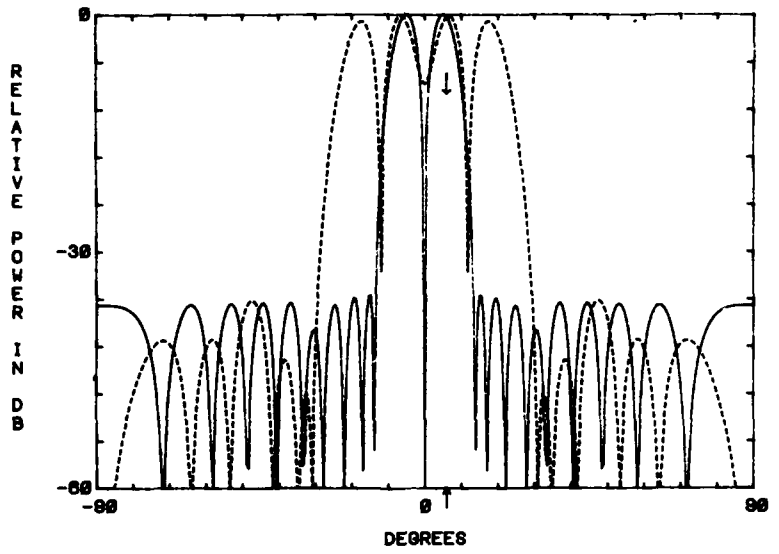

Figure 32d. Cancellation Beam From Phase-Only Nulling in the Sum and Difference Channels Simultaneously With a Jammer in the Mainbeam of the Difference Channel

Table 3. Nulling Results for Figures 27 to 32

Far Field Pattern Amplitude (dB below mainbeam)			
Amplitude Distribution	Jammer Angle	Errors	Far Field Amplitude
Taylor	33°	none	102
	33°	8-bit phase shifters	49
	33°	6-bit phase shifters	43
	33°	4-bit phase shifters	32
Bayliss	33°	none	101
	33°	8-bit phase shifters	50
	33°	6-bit phase shifters	40
	33°	4-bit phase shifters	31
Taylor	33°	No. 2 element failed	26
Taylor	29°	none	112
	70°	none	97
Taylor	29°	1 percent amplitude, 1° phase,	47
	70°	0.0001λ position, 8-bit phase shifters	40
Taylor	29°	2 percent amplitude, 4° phase,	16
	70°	0.001λ position, 8-bit phase shifters	42

7. CONCLUSIONS

A monopulse phased array similar to the one in Figure 11 requires an adaptive nulling technique that places nulls in its sum and difference far field patterns. One method of performing the nulling entails using one set of adaptive weights for the sum channel and another set for the difference channel (Figure 2). This method needs twice as many adaptive weights and more computations than nulling in a single channel. Unfortunately, nulling in one channel does not generate the same nulls in the other channel.

Sections 3 and 4 outlined techniques for placing nulls in sum and difference patterns. Of particular interest was simultaneous nulling in the sum and difference channels using one set of adaptive weights shared by the two channels. This method offers the advantage of halving the number of adaptive weights needed in methods using separate sets of weights for each channel. The disadvantages of the techniques are that the number of degrees of freedom are also cut in half. Since phased array

radars usually have many elements, hence can have many degrees of freedom, reducing the adaptive degrees of freedom by 50 percent will not appreciably affect the radar's antijamming, detecting, or tracking functions. However, the hardware savings are substantial.

The problem of practical implementation of the simultaneous nulling technique needs further investigation. The technique described does not employ feedback to adjust the nulls for the nonideal antenna pattern. The technique most be modified to incorporate a feedback-control system to adjust the adaptive weights. One way to change the algorithm is to adaptively adjust the cancellation beams until they are at the same height as the nonideal pattern, rather than the ideal pattern. Now, when the cancellation beams and nonideal pattern are added, the resultant pattern will have a null in the desired direction.

The phase shifts required to place nulls in the antenna pattern are quite small and prone to component errors. Phase shifter quantization is probably the major factor limiting the accuracy of nulling. Building digital phase shifters with more than 6 or 8 bit control lines is not a reasonable undertaking at this time. They would be too expensive to be practical and the last few bits would probably be in the noise level.

An alternative to the many-bit phase shifter is two separate sets of phase shifters. One set would make coarse adjustments for steering the main beam. They would have 4 bits or 22.5° accuracy. The other set would be phase shifters which could be accurately set between plus and minus 2°. These phase shifters would provide the small, accurate phase adjustments needed to place the nulls in the antenna patterns.

Besides the topic of practical implementation, other areas in simultaneous nulling need further investigation. For instance, partial adaptive nulling seems to be an appealing way to reduce the number of adaptive weights, while maintaining the nulling capability. This technique will probably work well theoretically. Another concern is mainbeam nulling. What are the limitations and how is the monopulse ratio affected? Finally, can simultaneous nulling be used without cutting the degrees of freedom in half? Perhaps there are sum and difference pattern distributions such that when a null is placed in one pattern, the null also appears in the other pattern. These are just a few of the areas of theoretical research that should be pursued.

This report has described the importance of nulling in both the sum and difference patterns of a monopulse antenna. Nulling in either the sum or difference channels will not place the same null in both far field patterns. It is theoretically possible to simultaneously place nulls in both far field patterns by adjusting one set of adaptive weights shared by the two channels. If this technique can be used on phased array antennas, there will be substantial savings in hardware. First, a practical way to implement the technique on actual phased array antennas is needed.

References

1. Elliot, Robert S. (1981) Antenna Theory and Design, Prentice-Hall, Inc., Englewood Cliffs, N.J.
2. Steinberg, B.D. (1976) Principles of Aperture and Array System Design, John Wiley, New York.
3. Skolnik, Merrill L. (1980) Introduction to Radar Systems, McGraw-Hill Book Co., New York.
4. Taylor, T.T. (1955) Design of line-source antennas for narrow beamwidth and low sidelobes, IRE Transactions-Antennas and Propagation, AP-3:16-28.
5. Bayliss, E.T. (1968) Design of monopulse antenna difference patterns with low sidelobes, The Bell System Technical Journal, May-June 1968:623-650.
6. Shore, R.A., and Steyskal, H. (1982) Nulling in Linear Array Patterns With Minimization of Weight Perturbations, RADC-TR-82-32, AD A118695.
7. Derusso, P.M., Roy, R.J., and Close, C.M. (1965) State Variables for Engineers, John Wiley & Sons, Inc., New York.
8. Baird, C.A., and Rassweiler, G.G. (1976) Adaptive nulling using digitally controlled phase-shifters, IEEE Trans. on Antennas and Propagation, 24(No. 5):638-649.
9. Brookner, E. (n.d.) Antenna array fundamentals. Taken from course notes from Microwave Journal Intensive Course, Practical Phased-Array Systems.

Appendix A

Computer System

The low sidelobe synthesis techniques and nulling algorithms were programmed in BASIC on the Tektronix 4052 computer. A diagram of the computer set up is shown in Figure A1. The Tektronix 4052 has 64K of memory and tape storage capability. To the left of the computer is the Tektronix 4663 plotter. It drew all the plots used in this report. On the right is a Tektronix 4631 hard copy unit and Tektronix 4641 printer.

Figure A2 shows a block diagram of the computer algorithm. First, data such as the number of elements and element spacing, are entered on the keyboard. Next, the program calculates the amplitude weights for either a uniform, Taylor, or Chebychev sum distribution and for either a uniform or Bayliss difference distribution. This part of the program models the low sidelobe synthesis techniques described in Section 2. Multiplying the zero factors together to obtain the polynomial p(s) is very inefficient. Only linear array distributions with up to 30 elements can be derived without taking excessive computer time.

After calculating the desired array distribution, the program enters into the nulling routines. The routine offers six different choices:

(1) Amplitude and phase nulling in sum channel,
(2) Amplitude and phase nulling in difference channel,
(3) Amplitude and phase nulling simuitaneously,
(4) Phase only nulling in sum channel,
(5) Phase only nulling in difference channel,
(6) Phase only nulling simultaneously.

The routine changes the quiescent sum and difference channels for one of the above choices. Both channels are assumed to share one set of adaptive weights. In cases 1 and 4 the adaptive weights are adjusted to place nulls in the sum channel. The difference channel receives the exact same weight change. For cases 2 and 5 the reverse holds true. In cases 3 and 6 the adaptive weights are adjusted to yield nulls simultaneously in the sum and difference channels. When the nulling routine is completed, the program stores the quiescent, adapted, and cancellation beam weights on tape. Next, the program calculates the far field pattern of any of the array weights stored on tape. The user interactively specifies the number of plots on the graph, the number of far field transform points on each plot, the angular extent of the graph and the normalization value. In this way, the output can be modified to obtain the necessary details. Finally, the computer draws the graph on the CRT and/or the plotter.

I wrote all parts of the program except for the complex inversion routine. That routine came from a Tektronix library tape.

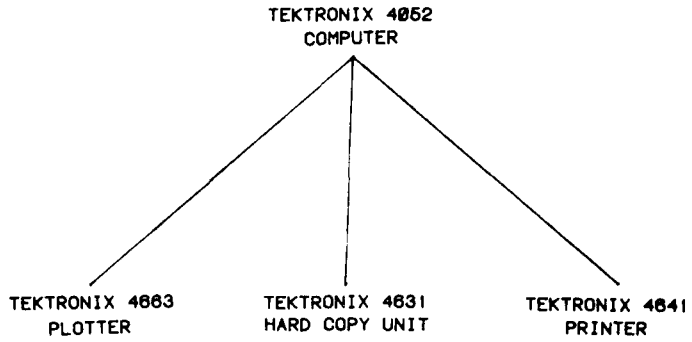

Figure A1. Block Diagram of the Computer Layout

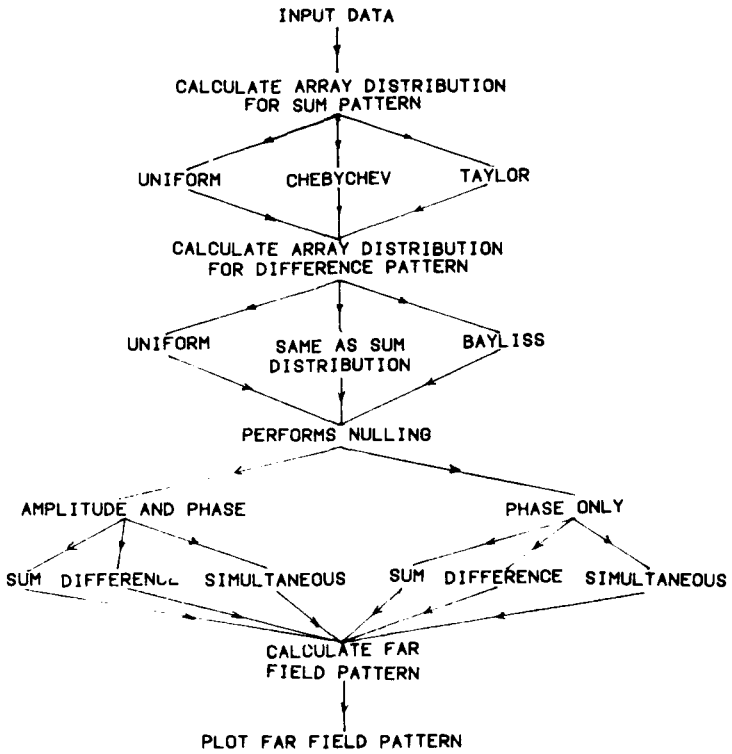

Figure A2. Block Diagram of the Computer Program

Appendix B

Effects of Errors on Sidelobe Levels

The following pages contain diagrams of RMS sidelobe level vs number of antenna elements for errors due to

(1) Random phase variations,
(2) Random amplitude variations,
(3) Phase shifter quantization,
(4) Random variations of element position,
(5) Element Failures.

These uncorrelated random errors are the inherent limitations to adaptive nulling. Better nulling requires better component tolerances, especially in low sidelobe antennas.

The errors in diagrams B1 to B15 were calculated from Eq. (135). A normal distribution was assumed for the phase, amplitude, and position errors. These errors have standard deviations of σ_{PH}, σ_A, and σ_p respectively. Element failures are represented by P_e, the probability of survival of the i^{th} radiating element. The effects of errors (including element failures) go down as the number of elements, gain, and aperture efficiency go up.

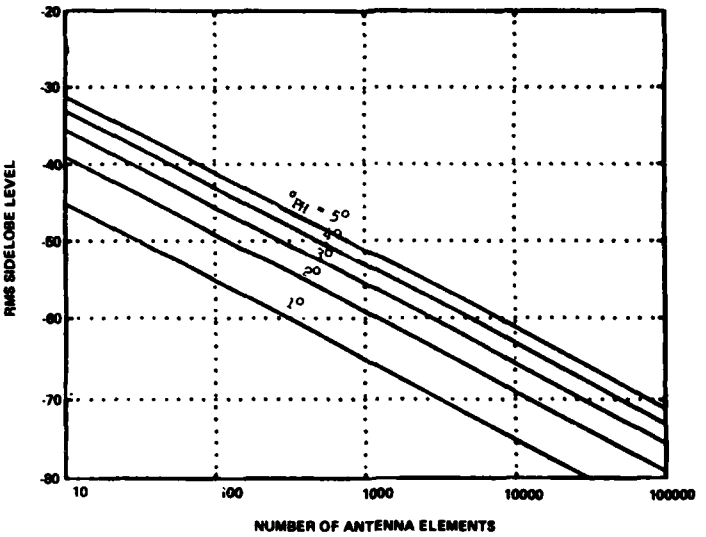

Figure B1. RMS Sidelobes Due to Random Phase Errors (η_T = 1.0)

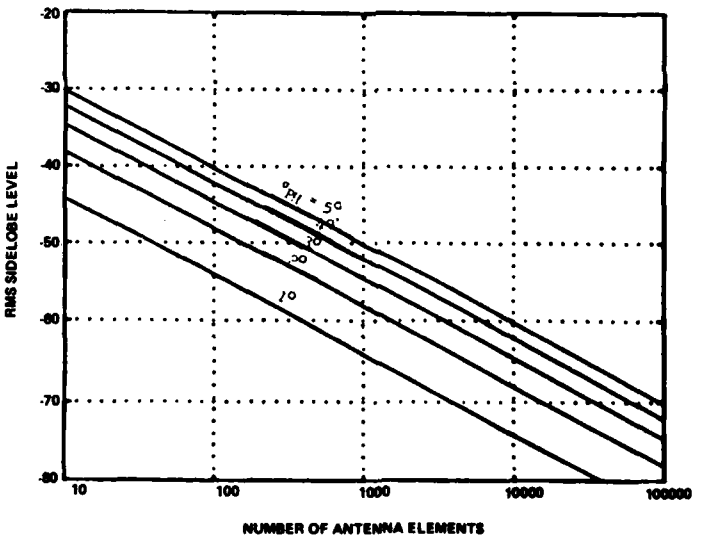

Figure B2. RMS Sidelobes Due to Random Phase Errors (η_T = 0.8)

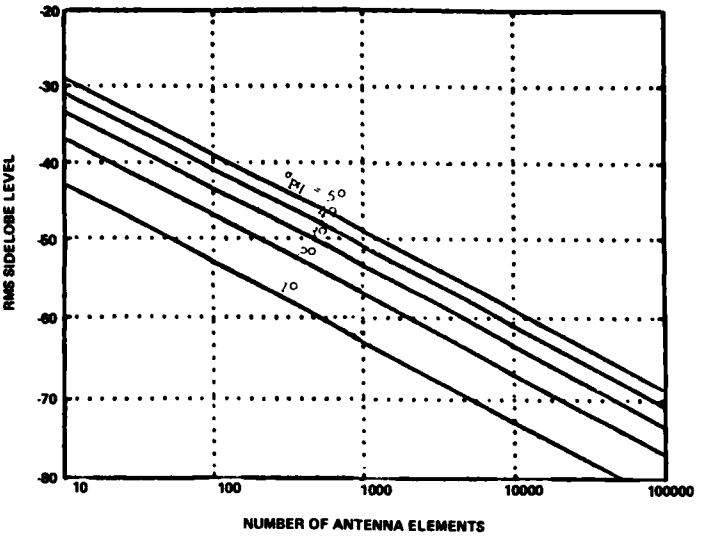

Figure B3. RMS Sidelobes Due to Random Phase Errors (η_T = 0.6)

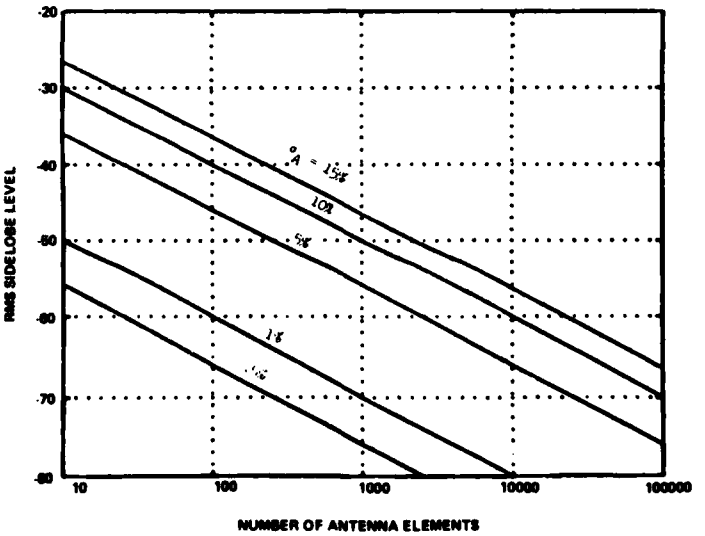

Figure B4. RMS Sidelobes Due to Random Amplitude Errors (η_T = 1.0)

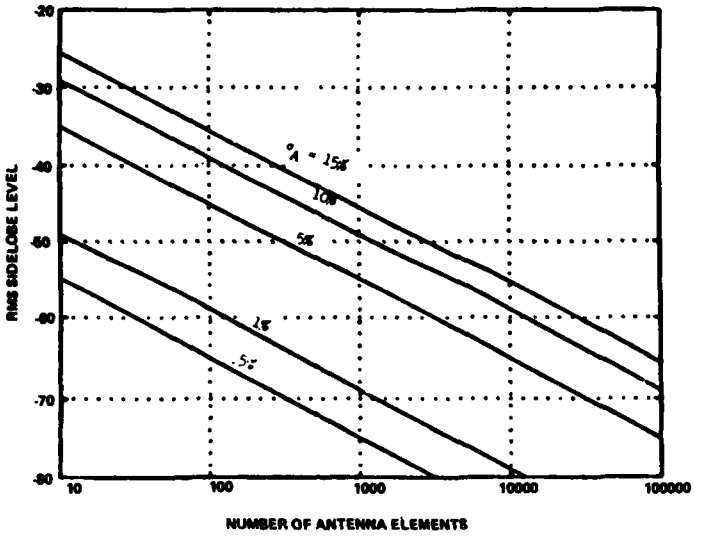

Figure B5. RMS Sidelobes Due to Random Amplitude Errors (η_T = 0.8)

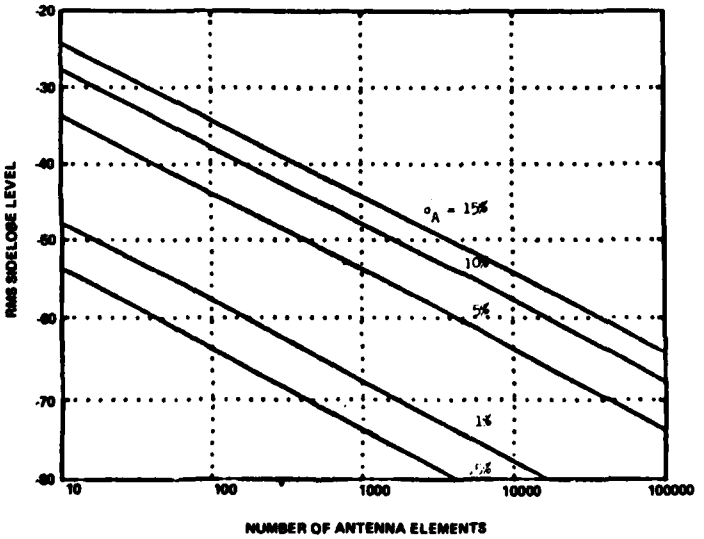

Figure B6. RMS Sidelobes Due to Random Amplitude Errors (η_T = 0.6)

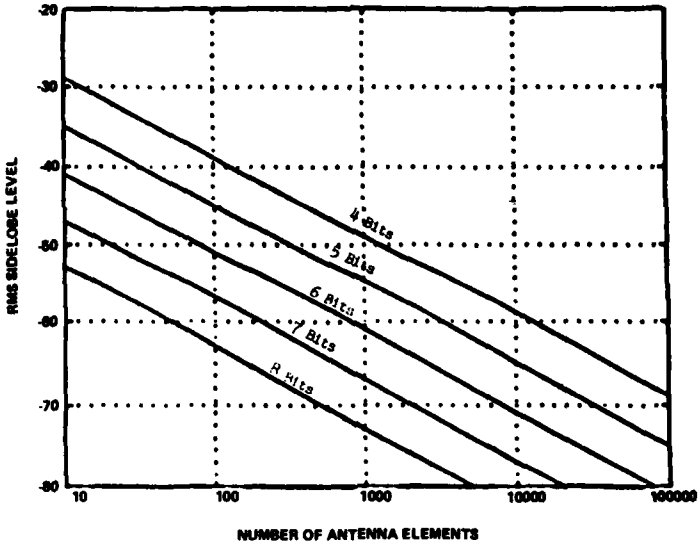

Figure B7. RMS Sidelobes Due to Quantization Errors (η_T = 1.0)

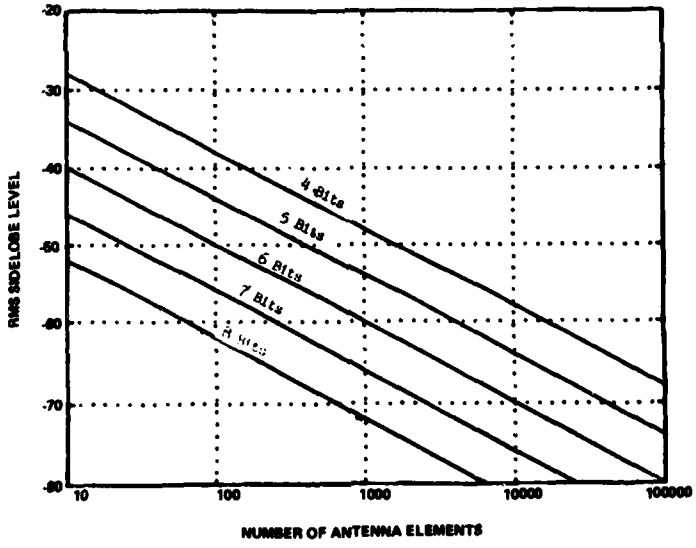

Figure B8. RMS Sidelobes Due to Quantization Errors (η_T = 0.8)

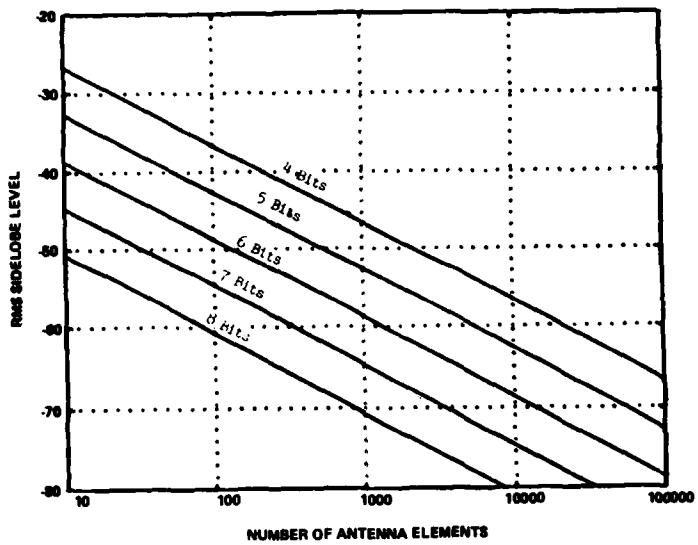

Figure B9. RMS Sidelobes Due to Quantization Errors (η_T = 0.6)

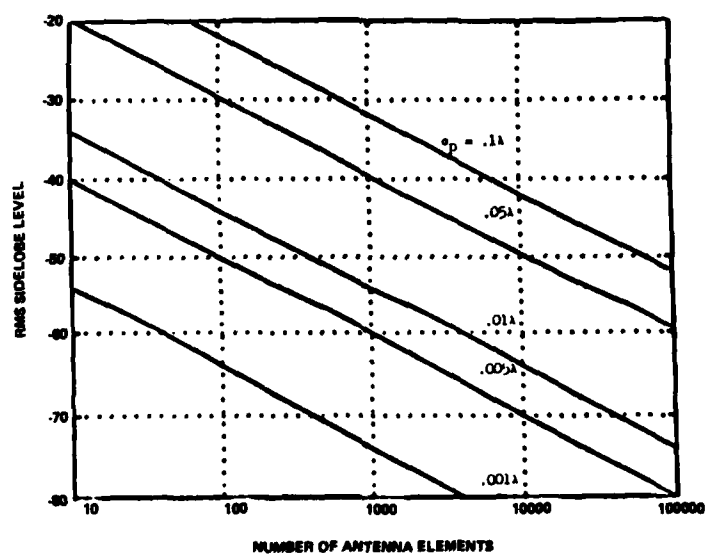

Figure B10. RMS Sidelobes Due to Element Position Errors (η_T = 1.0)

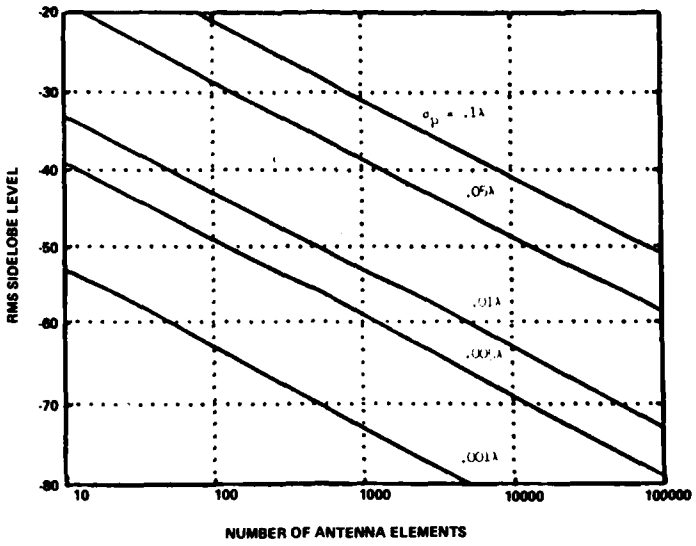

Figure B11. RMS Sidelobes Due to Element Position Errors (η_T = 0.8)

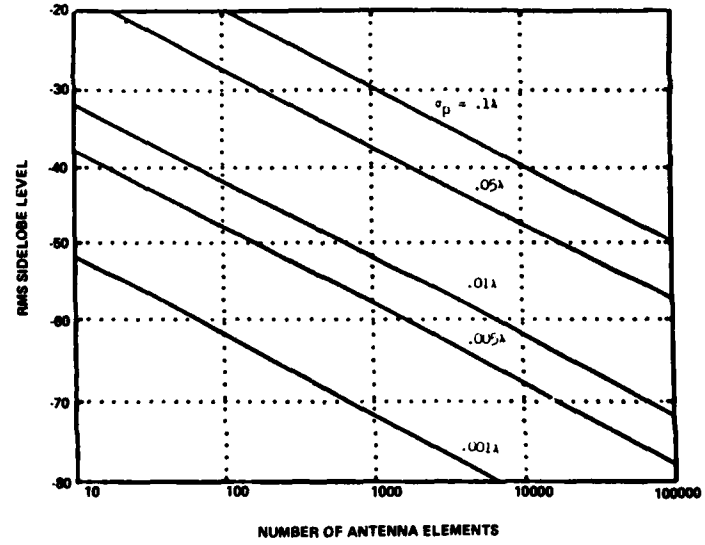

Figure B12. RMS Sidelobes Due to Element Position Errors (η_T = 0.6)

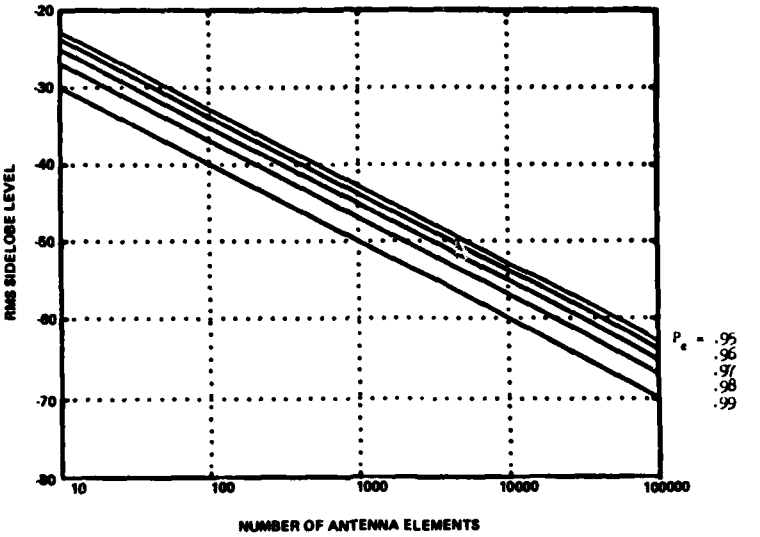

Figure B13. RMS Sidelobes Due to Element Failures (η_T = 1.0)

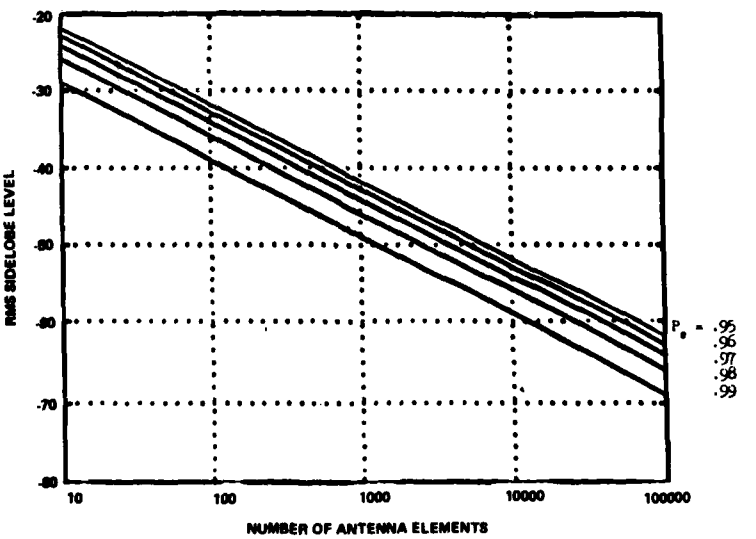

Figure B14. RMS Sidelobes Due to Element Failures (η_T = 0.8)

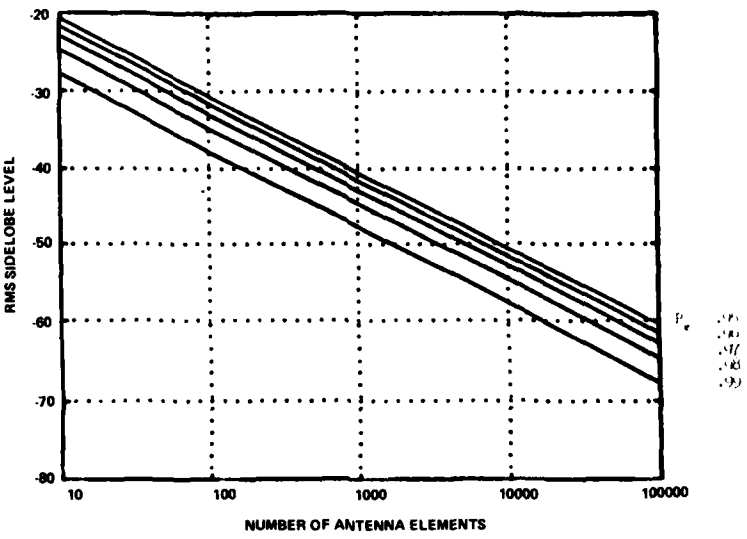

Figure B15. RMS Sidelobes Due to Element Failures (η_T = 0.6)